

# ScribblePrompt: Fast and Flexible Interactive Segmentation for Any Biomedical Image

Hallee E. Wong  
MIT CSAIL  
& MGH  
hallee@mit.edu

Marianne Rakic  
MIT CSAIL  
& MGH  
mrakic@mit.edu

John Guttag  
MIT CSAIL  
gutttag@mit.edu

Adrian V. Dalca  
MIT CSAIL  
& MGH, HMS  
adalca@mit.edu

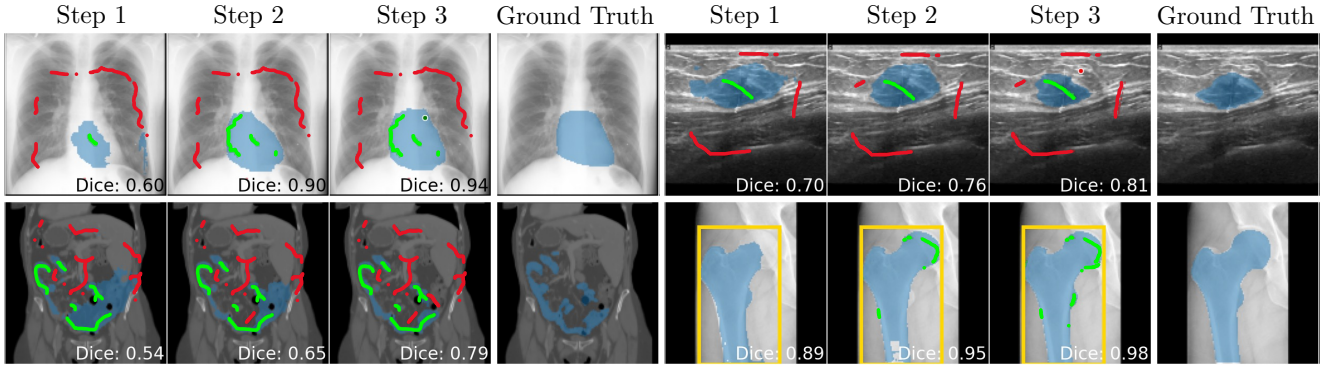


Figure 1. **ScribblePrompt** enables rapid iterative interactive segmentation of *unseen* tasks using bounding boxes, clicks, and scribbles. We show predictions from ScribblePrompt with iterative interaction steps on examples from datasets unseen during training. At each step, we visualize positive scribble and click inputs in green, negative scribble and click inputs in red, bounding box inputs in yellow, and the predicted segmentation in blue. Scribble thickness is enlarged for visual clarity. See Appendix for more examples.

## Abstract

Biomedical image segmentation is a crucial part of both scientific research and clinical care. With enough labelled data, deep learning models can be trained to accurately automate specific biomedical image segmentation tasks. However, manually segmenting images to create training data is highly labor intensive and requires domain expertise. We present *ScribblePrompt*, a flexible neural network based interactive segmentation tool for biomedical imaging that enables human annotators to segment previously unseen structures using scribbles, clicks, and bounding boxes. Through rigorous quantitative experiments, we demonstrate that given comparable amounts of interaction, *ScribblePrompt* produces more accurate segmentations than previous methods on datasets unseen during training. In a user study with domain experts, *ScribblePrompt* reduced annotation time by 28% while improving Dice by 15% compared to the next best method. *ScribblePrompt*'s success rests on a set of careful design decisions. These include a training strategy that incorporates both a highly diverse set of images and tasks, novel algorithms for simulated user interactions and labels, and a network that enables fast inference. We showcase

*ScribblePrompt* in an interactive demo and provide code at <https://scribbleprompt.csail.mit.edu>

## 1. Introduction

Biomedical image segmentation is an essential step in a wide range of biomedical research and clinical care pipelines. Deep learning has become the predominant method to automate existing segmentation tasks [55, 96, 111, 126]. Biomedical researchers and clinicians often encounter novel segmentation tasks involving either new regions of interest [144] or new image modalities [93, 116]. Unfortunately, supervised training of accurate models for new domains requires diverse images with careful annotations by skilled experts.

Most widely used interactive segmentation systems for biomedical imaging provide minimal, intensity-based, algorithmic assistance [143]. Despite a growing literature, learning-based systems are less widely used in practice, perhaps because they are generally focused on specific tasks or modalities, which limits their applicability [82, 102, 114, 133, 134, 152]. Recent vision foundation models target broad applicability, but require fine-tuning to the medical

domain [63, 135, 136, 153]. Most interactive segmentation models require specific interactions, like carefully placed clicks, making them easy to develop but difficult to use in practice. The result of these shortcomings is that existing learning-based models are not widely used in practice.

In this work, we present *ScribblePrompt*, a general model for interactive biomedical image segmentation that

1. enables users to rapidly and accurately accomplish any biomedical image segmentation task, outperforming state-of-the-art models, particularly for *unseen* labels and image types;
2. is flexible to different annotation styles, including bounding boxes, clicks, *and* scribbles,
3. is computationally efficient, enabling real-time inference, even on a single CPU.

To achieve this, we focused on design decisions aimed at ease of use and realistic interactions. To train our model, we started by gathering a large corpus of biomedical imaging datasets. We then designed task augmentation through synthesis strategies to encourage generalization to unseen tasks. Finally, we designed *new* interaction simulation strategies for training. The model itself uses an architecture optimized for efficient inference, to ensure real-time utility.

To evaluate ScribblePrompt, we compared its performance to that of existing interactive segmentation methods on datasets unseen during training. These experiments involved manually-collected scribbles, simulated interactions (Fig. 1), and a user study in which experienced annotators were asked to segment images. In the user study, ScribblePrompt reduced annotation time by 28% while increasing Dice by 15% compared to the next best method, the Segment Anything Model (SAM) [63]. Given similar amounts of interaction, ScribblePrompt achieved consistently better Dice scores than other methods.

We release an interactive tool, code, model weights, and our dataset of manually-collected scribbles at [scribbleprompt.csail.mit.edu](https://scribbleprompt.csail.mit.edu). We will also release new multi-annotator segmentation labels created using ScribblePrompt for select datasets.

## 2. Related Works

**Interactive Biomedical Image Segmentation.** Early research into interactive segmentation of biomedical images focused on traditional intensity-based methods [17, 26, 41, 129, 143]. Recent deep-learning based techniques [82, 102, 133, 134] use human interaction to improve the accuracy of segmentation tasks where labelled data exists, but fully-automatic segmentation methods fail to produce accurate segmentations. This approach assumes that the model will be used to perform the same segmentation task(s) it was trained on, leading to domain-specific solutions [7, 77, 98, 108, 132, 134]. A few methods generalize

to new, but similar, classes [114] and modalities [82, 133] to those seen in training. In contrast, ScribblePrompt is designed to help annotators segment a wide range of biomedical images and (potentially unseen) tasks at inference time.

**Foundation Models.** Recent vision foundation models employ prompting to enable generalization to new tasks. These models, trained on large collections of (natural) image data, segment potentially-unseen structures specified by spatial prompts [63, 153], text descriptions [63, 106, 153], or examples [20, 27, 135, 136]. Some of these models can be used for interactive segmentation with spatial prompts.

Fine-tuning models initially developed using natural images is often unhelpful for *specific* tasks in the biomedical imaging domain, compared to training from scratch [107]. The Segment Anything Model (SAM) [63], a foundation model trained on natural images, performs well at biomedical image segmentation tasks with clear boundaries (*e.g.* organ segmentation in abdominal CT), but performs poorly on tasks and modalities involving more subtle delineations (*e.g.* deep structures in Brain MRI) [45, 51, 92, 120]. Several recent or concurrent papers fine-tune SAM for specific biomedical tasks or modalities [50, 60, 75, 99, 131, 145]. A few fine-tune SAM to segment biomedical images from multiple-modalities with bounding boxes [84], clicks [138] or both [24]. We show in our experiments that these models don't perform well on many *unseen* tasks and are limiting in their required interactions.

Several natural image methods simulate *iterative* user interactions and condition the model on previous predictions to train a single network to make the initial prediction and perform refinement [18, 35, 63, 78, 122, 123]. This approach is appropriate for natural images where there is ample data and typically one modality. However, such methods have not previously been developed for the biomedical imaging domain, which is more fragmented because of specialized regions of interest and different modalities. We use iterative ideas in ScribblePrompt, but we facilitate iterative interactive segmentation of unseen biomedical imaging tasks.

**User Interaction.** Users can prompt interactive segmentation systems in many different ways, such as bounding boxes [13, 63, 108, 113, 133, 141], scribbles [23, 132, 134], or clicks [13, 78, 82, 123, 134]. Few interactive segmentation models incorporate multiple types of inputs. Some works have explored training with more specialized types of clicks [146], such as extreme points [87, 112], interior margin points [82], and center clicks [123, 140], to maximize the information per interaction. Specialized interactions often require more user time, and models trained only with such interactions are less robust to deviations from the interaction protocol [13, 123, 141]. In contrast, we focus on a user-friendly model that performs well under a variety of interaction scenarios.

Scribbles are an intuitive form of interaction, however few interactive segmentation works employ them, because acquiring *realistic* scribbles for training and evaluation is challenging. Previous deep-learning models trained for scribble-based segmentation either relied on collecting large datasets of manually drawn scribbles [70, 73, 152] or simplistic approaches such as sampling random points [6, 9, 134] or Bezier curves [3]. One work has explored simulating more complex scribbles for natural image segmentation [23]. We build on these concepts to create a new scribble simulation engine for training and evaluation.

### 3. ScribblePrompt Approach

We present an interactive segmentation method that can generalize to new biomedical imaging modalities and regions of interest, while staying focused on practical usability. We describe the problem formulation, and present the important aspects of the ScribblePrompt framework: (i) simulation of realistic and flexible interactions during training, (ii) augmentation with synthetic labels during training to encourage generalization, and (iii) an efficient architecture for real-time interaction. We show an overview of training in Fig. 3 and 4.

#### 3.1. Problem Formulation

Let  $t$  be a segmentation task consisting of image and segmentation pairs,  $\{(x^t, y^t)_j\}_{j=1}^N$ . At step  $i$ , given an image  $x^t$ , a set of user interactions  $u_i$ , and previous prediction  $\hat{y}_{i-1}^t$ , we learn function  $f_\theta(x^t, u_i, \hat{y}_{i-1}^t)$  with parameters  $\theta$  that produces a segmentation  $\hat{y}_i$ . The set of interactions  $u_i$ , which may include positive or negative scribbles, positive or negative clicks, and bounding boxes, is provided by a user who has access to the image  $x^t$  and previous prediction  $\hat{y}_{i-1}^t$ .

We minimize the difference between the true segmentation  $y^t$  and each of the iterative predictions  $\hat{y}_1, \dots, \hat{y}_k$ ,

$$\mathcal{L}(\theta; \mathcal{T}) = \mathbb{E}_{t \in \mathcal{T}} \left[ \mathbb{E}_{(x^t, y^t) \in t} \left[ \sum_{i=1}^k \mathcal{L}_{Seg}(y^t, f_\theta(x^t, u_i, \hat{y}_{i-1}^t)) \right] \right], \quad (1)$$

where  $\mathcal{L}_{Seg}$  is a supervised segmentation loss.

During training, we sample a task  $t$  from training task collection  $\mathcal{T}$ , from which we sample an image  $x^t$ , and segmentation map  $y^t$ . We simulate a possible set of interactions  $u_i$  based on  $y^t$ , and predict  $\hat{y}_i^t = f_\theta(x^t, u_i, \hat{y}_{i-1}^t)$ . We simulate the next set of interactions  $u_{i+1}$  based on the error region  $\varepsilon_i^t = y^t - \hat{y}_i^t$ , and repeat for  $k$  iterations. In the following sections, we describe the core aspects of the framework: strategies for simulating  $u_i$ , collecting  $\mathcal{T}$ , sampling  $(x^t, y^t)$ , building  $f_\theta$ , and optimizing  $\mathcal{L}(\theta; \mathcal{T})$ .

#### 3.2. Prompt Simulation

To enable a practical, easy-to-use model, we encourage robustness to different types of user interactions  $u_i$ . We introduce algorithms for simulating scribbles, clicks, and bound-

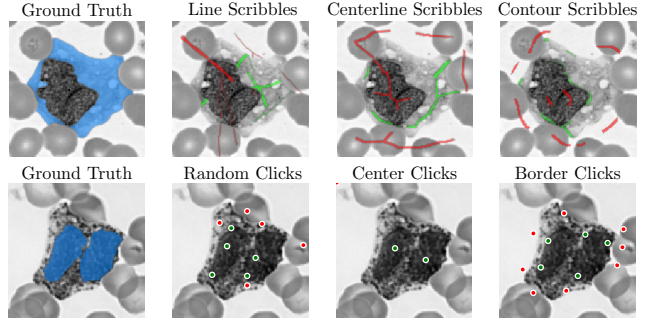


Figure 2. **Simulated scribbles and clicks.** Positive interactions (green) are simulated on the segmentation label  $y^t$  (blue), while negative interactions (red) are simulated on the background  $1 - y^t$ . Scribble thickness is enlarged for visual clarity.

ing box inputs during training. Each scribble and click strategy (Fig. 2) can be applied to a ground truth segmentation label  $y^t$  to simulate positive interactions, or to the background  $1 - y^t$  to simulate negative interactions. We simulate positive and negative correction scribbles or clicks by applying the same strategies to the false negative region  $\varepsilon_i^t > 0$  and false positive region  $\varepsilon_i^t < 0$  for error region  $\varepsilon_i^t$ .

**Scribbles.** Given binary mask  $y \in \{0, 1\}^{h \times w}$ , we simulate a scribble mask  $s \in [0, 1]^{h \times w}$  by first generating clean scribbles, and then corrupting them to account for user behavior and variability. We illustrate this process in Fig. 2 and Appendix B.1.1. To generate the clean scribbles, we start with one of these strategies:

- (i) **Line Scribbles:** We draw random lines by connecting two end points sampled from  $\{(u, v) | y_{uv} = 1\}$  (Fig. 8).
- (ii) **Centerline Scribbles:** We simulate scribbles in the center of label  $y$  using a thinning algorithm [147] that reduces the label to a 1-pixel wide skeleton (Fig. 9).
- (iii) **Contour Scribbles:** We simulate a rough contour of the desired segmentation within the boundaries of the mask (Fig. 10). We first blur the mask to reduce the size of the label such that  $\tilde{y} = \min(y, y \circ G_k)$ , where  $G_k$  is a Gaussian blur kernel. Then we apply a threshold  $\tilde{y} < h$  sampled in some intensity range  $h \sim U[\tilde{y}_{min}, \tilde{y}_{max}]$  and extract a contour inside the boundary of the mask.

To limit the size and complexity of the centerline and contour scribbles, we apply a random mask that breaks the scribbles into smaller parts. We generate the random mask by sampling a smooth noise image  $p$ , where each pixel is sampled independently from  $\mathcal{N}(\mu_p, \sigma_p^2)$ , applying Gaussian blur, and then thresholding it at  $\mu_p$ . We warp the resulting scribble mask  $s$  using a random deformation field  $\phi$  to vary the scribble shape and thickness. We ensure the resulting scribble is consistent with mask  $y$ , by multiplying the warped scribble mask  $s \circ \phi$  by  $y$ .

**Clicks.** Given a binary mask  $y \in \{0, 1\}^{h \times w}$ , we simulate  $n \sim U[n_{min}, n_{max}]$  clicks at a time using one of three strategies, illustrated in Fig. 2:

- (i) **Random clicks:** We randomly sample clicks from all pixels in the given region  $\{(u, v) | y_{uv} = 1\}$ .
- (ii) **Center clicks:** We sample clicks from the set of points at the center of each disconnected component of the label. First, we create a multi-label mask  $m \in \{1, \dots, C\}^{h \times w}$  identifying the  $C$  components of label  $y$ . We identify the center of each components using the euclidean distance transform [123, 140].
- (iii) **Interior border region clicks:** We sample clicks from a border region inside the boundary of the mask (Fig. 11). We first blur the mask  $y$  to reduce the size of the label such that  $\tilde{y} = \min(y, y \circ G_k)$  where  $G_k$  is a Gaussian blur kernel. We then sample click coordinates from  $\{(u, v) | \tilde{y}_{uv} \in [a, b]\}$ , where  $a, b \sim U[\tilde{y}_{min}, \tilde{y}_{max}]$  are thresholds sampled in some intensity range.

Since users are inclined to spread out their clicks, we impose a minimum separation of a few pixels between random clicks and border region clicks.

**Bounding Boxes.** We compute the minimum bounding box that encloses the label  $y^t$ , and enlarge each dimension by  $r \sim U[0, 20]$  pixels to account for human variability.

**Iterative Training (Fig. 3).** During the first step ( $i = 1$ ), we sample the combination of interactions and the number of initial positive and negative interactions  $n_{pos}, n_{neg} \sim U[n_{min}, n_{max}]$ . The initial interactions  $u_1$  are simulated using the ground truth label  $y^t$ . In subsequent steps, correction scribbles or clicks are sampled from the error region  $\varepsilon_{i-1}^t$  between the last prediction  $\hat{y}_{i-1}^t$  and the ground truth  $y^t$ . Since a user can make multiple corrections in each step, we sample  $n_{cor} \sim U[n_{min}, n_{max}]$  corrections (scribbles or clicks) per step.

### 3.3. Data

We build on large dataset gathering efforts like MegaMedical [20, 109] to compile a collection of 77 open-access biomedical imaging datasets for training and evaluation, covering over 54k scans, 16 image types, and 711 labels. The collection includes a diverse array of biomedical domains, such as eyes [49, 72, 85, 104, 125], thorax [105, 115, 117, 119, 121], spine [80, 117, 137, 150], cells [21, 22, 36, 37, 79, 151], skin [25], abdominal [15, 16, 46, 56, 59, 67, 68, 71, 76, 81, 86, 105, 110, 121, 124], neck [64, 97, 101, 103], brain [4, 10, 38, 47, 65, 66, 88, 89, 91, 121], bones [43, 117, 137], teeth [1, 53] and lesions [5, 121, 148, 149].

We define a 2D segmentation task as a combination of dataset, axis (for 3D modalities), and label. For datasets with multiple segmentation labels, we consider each label sepa-

rately as a binary segmentation task and for 3D modalities we use the slice with maximum label area and the middle slice from each volume. We provide more details on the data in Appendix C.

**Task Diversity.** During training we sample image, segmentation pairs hierarchically – by dataset and modality, axis, and then label – to balance training on datasets of different sizes. To increase the diversity of segmentation tasks, we apply data augmentation [20] to both the input image and sampled segmentation prior to simulating the user interactions.

**Synthetic Labels.** To limit overfitting to specific segmentation tasks, we introduce a mechanism to generate synthetic labels (Fig. 4). During training, for a given sample  $(x_0, y_0)$ , with probability  $p_{synth}$ , we replace  $y$  with a synthetic label  $y_{synth}$ . Given an image  $x_0$ , we generate a synthetic label  $y_{synth}$  by applying a superpixel algorithm [33] with scale parameter  $\lambda \sim U[1, \lambda_{max}]$  to partition the image into a multi-label mask of  $k$  superpixels  $z \in \{1, \dots, k\}^{n \times n}$ , and then randomly select a superpixel  $y_{synth} = \mathbb{1}(z = c)$ . We show examples in Fig. 14 and conduct experiments varying  $p_{synth}$ .

### 3.4. Network

Motivated by producing a practical tool, we primarily demonstrate ScribblePrompt using an efficient fully-convolutional architecture similar to a UNet [111]. We also demonstrate ScribblePrompt using a vision transformer-based architecture, SAM ViT-b [63]. We provide code and weights for both models at [scribbleprompt.csail.mit.edu](https://scribbleprompt.csail.mit.edu).

**ScribblePrompt-UNet.** We use an 8 layer CNN following a decoder-encoder structure similar to the popular UNet architecture [111] without Batch Norm. Each convolutional layer has 192 features and uses PReLU activation [44].

We encode each prompt type in an input channel. The input to ScribblePrompt-UNet has size  $5 \times h \times w$  consisting of the input image  $x^t$ , bounding box encoding, positive click/scribble encoding, negative click/scribble encoding, and the logits of the previous prediction  $\hat{y}_{i-1}^t$ . We encode bounding boxes in a binary mask that is 1 inside the box(es) and 0 everywhere else. We encode positive and negative clicks using binary masks, and combine them with the positive and negative scribble masks.

**ScribblePrompt-SAM.** We take the smallest SAM model (ViT-b) and fine-tune the decoder. SAM takes bounding box and click inputs as lists of  $(x, y)$  coordinates, and the low-resolution logits of the previous prediction  $\hat{y}_{i-1}$ . To adapt SAM for scribbles, we consider each positive/negative scribbled pixel as a positive/negative click.

**Loss.** We minimize eq. (1) where  $\mathcal{L}_{Seg}$  is a linear combination of soft Dice Loss [32] and Focal Loss [74]. In preliminary experiments (Appendix B.2), training with Soft Dice

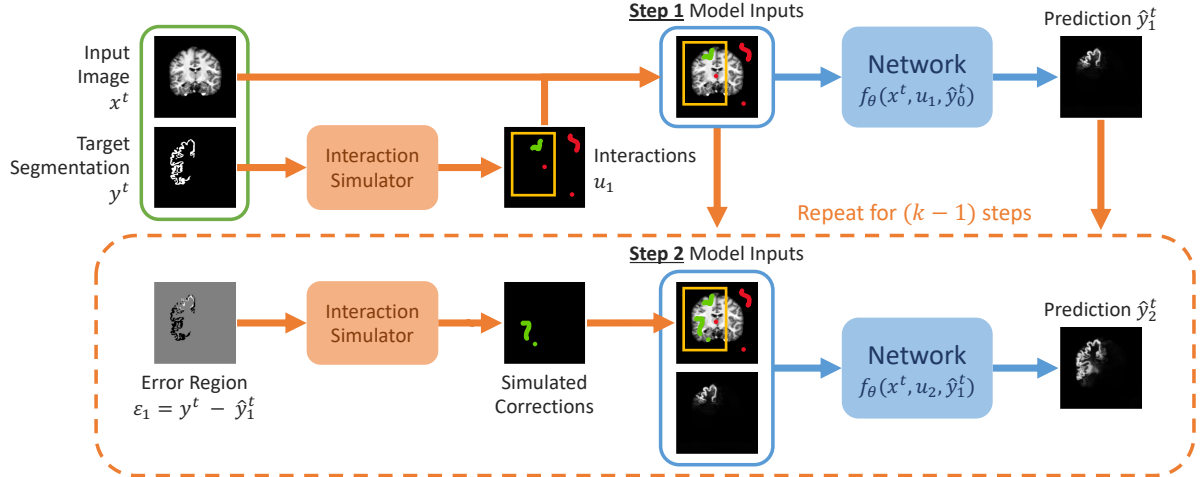


Figure 3. **Training.** We simulate  $k$  consecutive steps of interactive segmentation. Given an image segmentation pair  $(x^t, y^t)$ , we first simulate a set of initial interactions  $u_1$ , which may contain bounding boxes, clicks, and/or scribbles. We predict segmentation  $\hat{y}_1^t := f_\theta(x^t, u_1, \hat{y}_0^t)$  where the initial prediction  $\hat{y}_0^t$  is set to zeros. In the second step, we simulate corrections using the error region  $\epsilon_1$  between the previous prediction  $\hat{y}_1$  and ground truth  $y$ , and add them to the set of initial interactions  $u_1$  to get  $u_2$ . We predict segmentation  $\hat{y}_2 := f_\theta(x, u_2, \hat{y}_1)$  and repeat to produce a series of  $k$  iterative predictions,  $\hat{y}_1, \dots, \hat{y}_k$ . We learn  $\theta$  to minimize  $\sum_{i=1}^k \mathcal{L}_{seg}(y^t, \hat{y}_i)$ , the sum of losses between the target segmentation  $y^t$  and iterative predictions  $\hat{y}_1, \dots, \hat{y}_k$ .

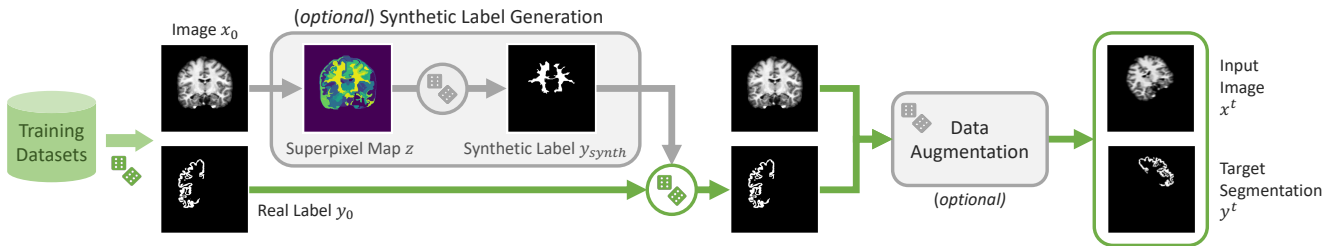


Figure 4. **Task sampling and augmentation.** During training, we sample an image and segmentation pair  $(x_0, y_0)$ . With probability  $p_{synth}$ , we replace  $y_0$  with a synthetic label  $y_{synth}$ . We generate  $y_{synth}$  by applying a superpixel algorithm to the image  $x_0$  to generate a map  $z$  of potential synthetic labels (superpixels), and then sampling one label. Finally, we apply random data augmentations to get  $(x^t, y^t)$ .

Loss [32] alone or a linear combination of Soft Dice Loss and Binary-Cross Entropy Loss resulted in slightly lower Dice scores.

## 4. Experimental Setup

We compare ScribblePrompt-UNet and ScribblePrompt-SAM to previous methods through experiments with manual scribbles, simulated interactions, and a user study with experienced annotators. Lastly, we report on inference runtime and ablation experiments.

**Data.** We use 65 (out of 77) datasets during training. We partition another nine datasets, ACDC [14], BUID [5], BTCV Cervix [68], DRIVE [125], HipXRy [43], PanDental [1], SCD [105], SpineWeb [150], and WBC [151], each into validation (used in model selection, but not training) and test (used only for final evaluation). Three additional datasets, TotalSegmentator [137], SCR [128], and COBRE [4, 29, 34],

were used only for final evaluation.

We report final results on 12 sets of data (the test splits of the 9+3 evaluation datasets). The evaluation datasets were not seen during training, and cover 608 tasks and 8 modalities, including unseen image types and unseen labels. We selected these 12 evaluation datasets to cover a variety of modalities (MRI, CT, ultrasound, fundus photography, microscopy) and anatomical regions of interest (brain, teeth, bones, abdominal organs, muscles, heart, thorax, cells), including both healthy anatomy and lesions.

**Training.** During training, we simulated five steps of interactive segmentation per example and set the maximum number of interactions per step to three. We set the minimum number of initial negative prompts to zero, and the minimum initial positive and correction prompts to one. During the first step, we sample the combination of prompt types (clicks, scribbles, bounding boxes) and then sample the number of positive and negative interactions for each type. In each subsequent steps,

we simulate either scribble corrections or click corrections with equal probability. We selected these values based on what we believe to be reasonable interactions for a user to perform.

**Baselines.** We compare to existing generalist methods for interactive segmentation, with a focus on methods developed for biomedical imaging.

**SAM** [63]: We evaluate the smallest (ViT-b) and largest (ViT-h) versions of the Segment Anything Model (SAM) trained on natural images. SAM takes bounding boxes, clicks, and the logits of the previous prediction as input.

**SAM-Med2D** [24]: SAM-Med2D is a SAM ViT-b model with additional adapter layers in the image encoder. SAM-Med2D was fine-tuned, using bounding boxes and iterative clicks as input, on a collection of biomedical imaging datasets containing 4.6M images and 19.7M segmentations. Following [24], we evaluate SAM-Med2D both with and without adapter layers.

**MedSAM** [84]: MedSAM is a SAM ViT-B model fine-tuned with bounding box prompts on a collection of biomedical imaging datasets containing 1.5M image segmentation pairs. We evaluate MedSAM with bounding boxes only, because we found it to perform poorly when given point or mask prompts (Fig. 24).

**MIDeepSeg** [82]: MIDeepSeg is an interactive segmentation framework designed to generalize to unseen tasks on medical images. MIDeepSeg takes interior margin points (positive clicks) as initial inputs. It crops the image based on those points and uses a CNN to make an initial prediction. Given additional clicks, the prediction can be refined using conditional random fields. We evaluate the pre-trained model, which was developed on placenta T2 MRI.

## 5. Evaluation

We evaluate all methods using both manual and simulated interactions, with a focus on scribbles. Simulated interactions enable us to test on a large volume of images and tasks. However, simulations do not always match user behavior. We address this by (1) collecting a diverse dataset of manual scribbles for evaluation, and (2) conducting an interactive user study.

### 5.1. Manual Scribbles

**Setup.** We evaluate on two datasets of manual scribbles. First, we collected a dataset (MedScribble) of manual scribbles from three annotators for seven segmentation tasks from unseen datasets, with a total of 31 examples. The annotators were shown five training examples with the ground truth segmentation per task and instructed to draw positive and negative scribbles to indicate the region of interest on new images. We provide more details on MedScribble in Appendix E. Second, we used 380 slices from the ACDC

dataset [14], which has scribble annotations for three labels and background.

In this evaluation, we make a prediction given a set of positive and negative scribbles, simulating a non-iterative scenario where the annotator draws several scribbles before running inference. We evaluate accuracy using Dice score [32] and 95th percentile Hausdorff Distance [52]. Since MIDeepSeg’s initial prediction network only takes positive inputs, we report results on both MIDeepSeg’s initial prediction from the positive scribbles, and after applying MIDeepSeg’s refinement procedure using the negative scribbles as corrections. For SAM and variants fine-tuning SAM on clicks, we convert each scribble to a series of points. For MedSAM, we fit a bounding box to the positive scribbles.

**Results.** ScribblePrompt-UNet and ScribblePrompt-SAM produce the most accurate segmentations in a single step of manual scribbles on both our manual scribbles dataset and the ACDC scribbles dataset (Tab. 1). We show example predictions in Fig. 5 and Appendix E.

SAM and SAM-Med2D do not generalize well to scribble inputs (which they were not trained for). MedSAM has better predictions than other SAM baselines using the SAM architecture, however it is not able to make use of the negative scribbles and thus often misses segmentations with holes in them (Fig. 5). The initial predictions from MIDeepSeg’s network are poor, but improve after applying the refinement procedure.

### 5.2. Simulated Interactions

**Setup.** We use our interaction simulator to evaluate the performance of ScribblePrompt and baselines with iterative scribbles across the 12 evaluation sets.

For scribble-focused prompting procedures, we use:

- **Line Scribbles:** Three positive line scribbles and three negative line scribbles to start, followed by one correction line scribble at each step.
- **Centerline Scribbles:** One positive and one negative centerline scribble to start, followed by one correction centerline scribble at each step.
- **Contour Scribbles:** One positive and one negative contour scribble to start, followed by one correction contour scribble at each step.

We limit each scribble to cover a maximum of  $w$  pixels, where  $w$  is the maximum dimension of the image. For centerline and contour scribbles, a scribble might contain multiple disconnected components.

For click-focused prompting procedures, we use:

- **Center Clicks:** One positive click in the center of the largest component to start, followed by one (positive or negative) correction click per step in the center of the largest component of the error region.
- **Random Clicks:** One random positive click to start, fol-

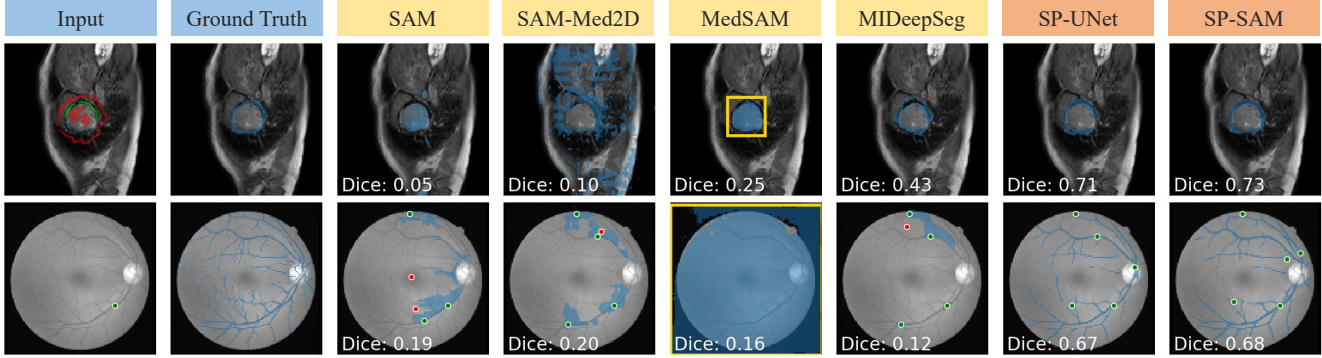


Figure 5. **Example predictions.** SP = ScribblePrompt. Top: predictions after one step of manual scribbles. Bottom: predictions after five steps of simulated interactions (one center click followed by one center correction click per step). See the Appendix E,F for more examples.

Table 1. **Manual scribbles.** We report mean Dice and HD95 with 95% CI of segmentations predicted from manually-collected scribbles. Best and second best are highlighted.

Model	MedScribble (n=93)		ACDC (n=2,130)	
	↑ Dice Score	↓ HD95	↑ Dice Score	↓ HD95
SAM (ViT-b)	0.40 ± 0.05	32.58 ± 3.80	0.20 ± 0.01	108.39 ± 0.85
SAM (ViT-h)	0.56 ± 0.05	14.61 ± 3.18	0.42 ± 0.02	59.78 ± 2.02
SAM-Med2D w.o. adapter	0.52 ± 0.05	30.34 ± 3.29	0.16 ± 0.01	107.25 ± 1.12
SAM-Med2D w/ adapter	0.30 ± 0.06	19.04 ± 3.63	0.17 ± 0.02	41.01 ± 3.04
MIDeepSeg	0.68 ± 0.04	6.94 ± 1.06	0.58 ± 0.01	5.78 ± 0.26
MIDeepSeg w/ refinement	0.81 ± 0.03	3.10 ± 0.67	0.73 ± 0.01	2.71 ± 0.18
MedSAM (box)	0.70 ± 0.04	7.54 ± 1.35	0.70 ± 0.02	3.53 ± 0.28
<b>ScribblePrompt-SAM</b>	0.87 ± 0.02	2.61 ± 0.84	0.77 ± 0.01	4.17 ± 0.32
<b>ScribblePrompt-UNet</b>	0.84 ± 0.02	2.92 ± 0.88	0.84 ± 0.01	1.80 ± 0.11

lowed by one (positive or negative) correction click per step, randomly sampled from the error region.

- **Random Warm Start:** Three random positive clicks and three random negative clicks to start, followed by one (positive or negative) correction click per step in the center of the largest component of the error region.

For each example and interaction procedure, we simulate a series of iterative interactions with five random seeds. Since MIDeepSeg cannot make accurate predictions with only a few clicks, we exclude it from simulations that start with a single click. For MedSAM, we show results for a bounding box prompt.

**Results.** Fig. 6 shows that both versions of ScribblePrompt outperform baseline methods for all simulated interaction procedures at all numbers of interactions. We show examples with simulated interactions in Fig. 1 and Fig. 5 (bottom). We show results with similar trends using bounding boxes and by dataset with fully-supervised baselines in Appendix F.

**Discussion.** Comparing the simulated scribble and click results (Fig. 6) highlights the efficiency of scribble-based in-

teractions. Both ScribblePrompt models reach an average Dice above 0.8 in two scribble steps. It takes five steps of carefully-placed center clicks or eight random clicks to reach the same average Dice score with ScribblePrompt-SAM.

Although SAM-Med2D was trained on a large biomedical imaging collection, it does not perform as well as SAM at refining its predictions on held-out evaluation sets. MedSAM only uses bounding box prompts and is not able to refine predictions, limiting its performance and usability.

### 5.3. User Study

To assess the practical utility of ScribblePrompt, we conducted a user study with experienced annotators. We compare ScribblePrompt-UNet to SAM (ViT-b). We selected ScribblePrompt-UNet for the user study because it had similar performance and lower latency compared to ScribblePrompt-SAM. We selected SAM (ViT-b) because it had the highest Dice score in our experiments with clicks and lower latency than the next closest baseline, SAM (ViT-h).

**Setup.** Study participants ( $n = 16$ ) were neuroimaging re-

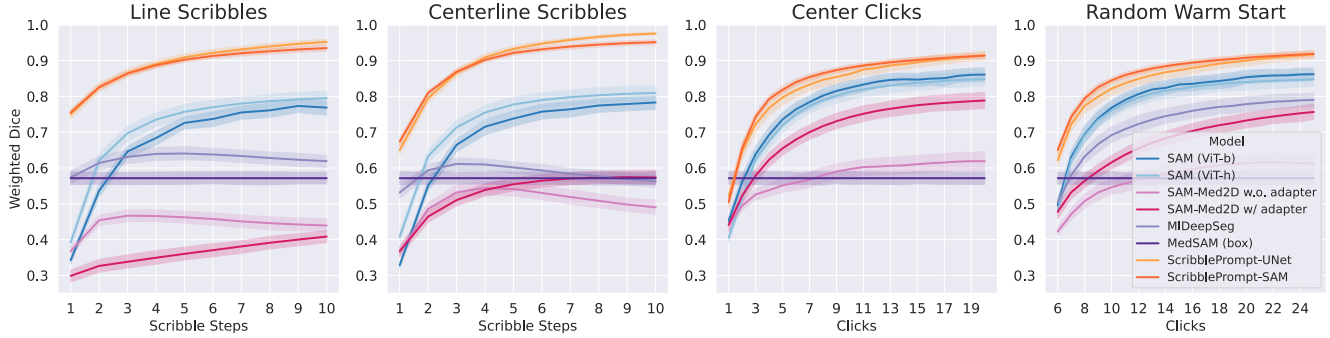


Figure 6. **Simulated clicks and scribbles.** We simulate interactions following three scribble protocols and three click protocols. We show more results, with similar trends, in Appendix F.2 (Fig. 21).

Table 2. **User study.** We report means and standard deviations for Dice score, HD95 and total time per segmentation, as well as the median (and max) number of times the participants ( $n = 16$ ) refreshed the prediction.

	SAM (ViT-b)	ScribblePrompt-UNet
Dice Score ( $\uparrow$ )	0.73 $\pm$ 0.30	0.84 $\pm$ 0.13
HD95 ( $\downarrow$ )	16.1 $\pm$ 37.1	4.5 $\pm$ 9.1
Sec./task ( $\downarrow$ )	131.7 $\pm$ 168.5	94.2 $\pm$ 89.0
Iter./task ( $\downarrow$ )	6 (47)	3 (19)

searchers at an academic hospital. They used each model to segment a series of nine test images from different evaluation datasets. For each segmentation task, the participants were shown the target segmentation and were asked to prompt the model until the predicted segmentation closely matched the target, or they could no longer improve the prediction. We provided participants with the target segmentation to disentangle the cognitive process of identifying the region of interest from prompting the model to achieve the desired segmentation. We provide additional details and visualizations in Appendix G.

**Results.** Participants produced more accurate segmentations (0.84 vs. 0.73 Dice;  $p = 0.001$  using a paired t-test) using ScribblePrompt (Tab. 2). Participants spent  $\approx 1.5$  minutes per segmentation on average using ScribblePrompt, compared to over 2 minutes per segmentation with SAM ( $p = 0.02$  using a paired t-test). While using ScribblePrompt, participants updated the prediction fewer times before being satisfied with the segmentation.

Upon completion, 15 out of 16 participants reported they preferred using ScribblePrompt to SAM and one participant had no preference. All participants reported it was easier to achieve the target segmentation using ScribblePrompt compared to SAM. 93.8% of participants reported ScribblePrompt was better than SAM at refining its predictions in

response to scribbles. 87.5% of participants preferred using ScribblePrompt over SAM for clicks.

**Discussion.** The most common factors that influenced participant preference for ScribblePrompt were 1) being able to get accurate predictions from multiple types of prompts, including scribbles and 2) responsiveness to their corrections, which enabled fine-grained control over the next prediction. For some tasks, such as retinal vein segmentation, SAM was unable to make accurate predictions even with many corrections (Fig. 35). As a result, there was more variability in Dice score and time per segmentation, for SAM than ScribblePrompt.

## 5.4. Inference Runtime

**Setup.** We evaluate computational efficiency by measuring inference time on a single CPU for one prediction with a scribble input covering 128 pixels. Performance on a CPU reflects practical utility. Because of a variety of barriers such as protected health information, users may not be able to send their data to a server for computation, and must rely on local, most often CPU-only, computing.

**Results.** On a single CPU, ScribblePrompt-UNet requires  $0.27 \pm 0.04$  sec per prediction, enabling the model to be used in real-time even in low-resource environments. The next most accurate model (Fig. 6), SAM ViT-h, requires over 2 minutes per prediction on a CPU ( $130.79 \pm 7.96$  s). SAM ViT-b takes  $13.59 \pm 0.77$  seconds per prediction. We report results for all baselines and on GPU hardware with similar trends in Appendix H.

Its efficient fully-convolutional architecture gives ScribblePrompt-UNet low latency inference. With SAM, latency scales with the number of interactions because each point is encoded as a 256-dimensional vector embedding. For ScribblePrompt-UNet, clicks and scribbles are encoded in masks, so inference time (per prediction) is constant with the number of interactions.



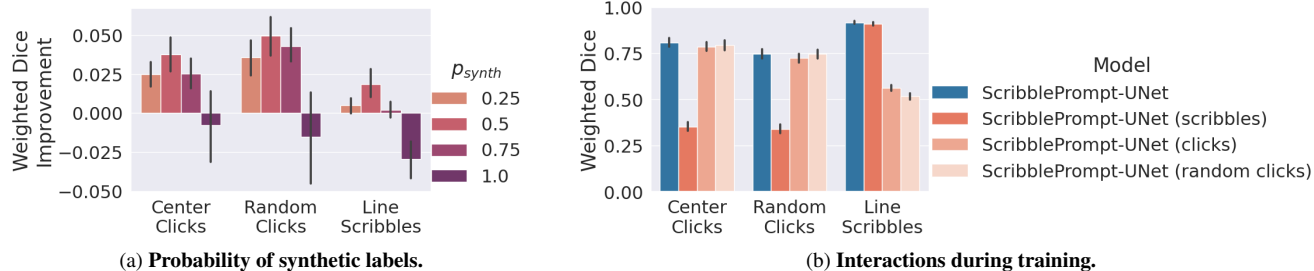


Figure 7. **Ablations.** We report Dice after five steps of simulated interactions following three inference-time interaction procedures. Error bars show 95% CI. (a) shows mean change in Dice relative to ScribblePrompt-UNet trained without any synthetic labels ( $p_{synth} = 0$ ).

## 6. Ablations

We conduct two ablations of important design decisions: (1) synthetic label inputs used during training, and (2) types of prompts simulated during training. We report results on the validation splits of nine datasets unseen during training.

### 6.1. Synthetic Labels

**Setup.** We trained ScribblePrompt-UNet with different values of  $p_{synth}$ , the probability of sampling a synthetic label.

**Results.** Fig. 7a shows the effect of varying the percentage of synthetic labels during training for ScribblePrompt-UNet. Training with both real and synthetic labels improves generalization to new datasets, compared to training with only real labels. Using  $p_{synth} = 0.5$  results in the highest Dice. Training with *only* synthetic labels results in worse Dice scores. We show similar results for ScribblePrompt-SAM and other interaction procedures in Appendix I.1.

### 6.2. Prompt Types

**Setup.** We evaluate ScribblePrompt-UNet models trained with different combinations of prompts, compared to the complete ScribblePrompt-UNet:

- **ScribblePrompt-UNet (scribbles)** trained on boxes and scribbles.
- **ScribblePrompt-UNet (clicks)** trained on boxes and clicks.
- **ScribblePrompt-UNet (random clicks)** trained on boxes and random clicks.

**Results.** Fig. 7b shows ScribblePrompt-UNet trained with scribbles, clicks and bounding boxes predicts segmentations more accurately than do ablated versions of ScribblePrompt-UNet. We show results for other interaction procedures with similar trends in Appendix I.2.

## 7. Conclusion

We present ScribblePrompt, a practical framework for interactive segmentation that enables users to segment diverse

medical images with scribbles, clicks, and bounding boxes. We introduce methods for simulating realistic user interactions and generating synthetic labels. These methods enable us to train models that generalize to unseen segmentation tasks and datasets. ScribblePrompt is more accurate than existing baselines, and ScribblePrompt-UNet is computationally efficient, even on a CPU. Our user study shows that nearly all users prefer ScribblePrompt and achieve segmentations with 15% higher Dice with less effort than the next most accurate baseline. ScribblePrompt promises to significantly reduce the burden of manual segmentation in biomedical imaging.

## 8. Acknowledgements

This work was supported in part by funding from Quanta Computer Inc., the Eric and Wendy Schmidt Center at the Broad Institute of MIT and Harvard and the Wistron Corporation. Research reported in this paper was supported by the National Institute of Biomedical Imaging and Bioengineering of the National Institutes of Health under award number R01EB033773. Much of the computation resources required for this research was performed on computational hardware generously provided by the Massachusetts Life Sciences Center.

## References

- [1] Amir Hossein Abdi, Shohreh Kasaei, and Mojdeh Mehdizadeh. Automatic segmentation of mandible in panoramic x-ray. *Journal of Medical Imaging*, 2(4):044003, 2015. 4, 5, 7
- [2] Abubakar Abid, Ali Abdalla, Ali Abid, Dawood Khan, Abdulrahman Alfozan, and James Y. Zou. Gradio: Hassle-free sharing and testing of ML models in the wild. *CoRR*, abs/1906.02569, 2019. 7, 11
- [3] Eirikur Agustsson, Jasper R. Uijlings, and Vittorio Ferrari. Interactive Full Image Segmentation by Considering All Regions Jointly. In *2019 IEEE/CVF Conference on Computer Vision and Pattern Recognition (CVPR)*, pages 11614–11623, Long Beach, CA, USA, 2019. IEEE. 3
- [4] C. J. Aine, H. J. Bockholt, J. R. Bustillo, J. M. Cañive,

- A. Caprihan, C. Gasparovic, F. M. Hanlon, J. M. Houck, R. E. Jung, J. Lauriello, J. Liu, A. R. Mayer, N. I. Perrone-Bizzozero, S. Posse, J. M. Stephen, J. A. Turner, V. P. Clark, and Vince D. Calhoun. Multimodal Neuroimaging in Schizophrenia: Description and Dissemination. *Neuroinformatics*, 15(4):343–364, 2017. 4, 5, 19
- [5] Walid Al-Dhabyani, Mohammed Goma, Hussien Khaled, and Aly Fahmy. Dataset of breast ultrasound images. *Data in Brief*, 28:104863, 2020. 4, 5, 16
- [6] Muhammad Asad, Lucas Fidon, and Tom Vercauteren. ECONet: Efficient Convolutional Online Likelihood Network for Scribble-based Interactive Segmentation. In *International Conference on Medical Imaging with Deep Learning*, pages 35–47. PMLR, 2022. arXiv:2201.04584 [cs, eess]. 3
- [7] Alessia Atzeni, Loic Peter, Eleanor Robinson, Emily Blackburn, Juri Althonayan, Daniel C. Alexander, and Juan Eugenio Iglesias. Deep active learning for suggestive segmentation of biomedical image stacks via optimisation of Dice scores and traced boundary length. *Medical Image Analysis*, 81, 2022. 2
- [8] Jimmy Lei Ba, Jamie Ryan Kiros, and Geoffrey E Hinton. Layer normalization. *arXiv preprint arXiv:1607.06450*, 2016. 1
- [9] Junjie Bai and Xiaodong Wu. Error-Tolerant Scribbles Based Interactive Image Segmentation. In *2014 IEEE Conference on Computer Vision and Pattern Recognition*, pages 392–399, Columbus, OH, USA, 2014. IEEE. 3
- [10] Ujjwal Baid, Satyam Ghodasara, Suyash Mohan, Michel Bilello, Evan Calabrese, Errol Colak, Keyvan Farahani, Jayashree Kalpathy-Cramer, Felipe C Kitamura, Sarthak Pati, et al. The rsna-asnr-miccai brats 2021 benchmark on brain tumor segmentation and radiogenomic classification. *arXiv preprint arXiv:2107.02314*, 2021. 4, 6
- [11] Spyridon Bakas, Hamed Akbari, Aristeidis Sotiras, Michel Bilello, Martin Rozycki, Justin S Kirby, John B Freymann, Keyvan Farahani, and Christos Davatzikos. Advancing the cancer genome atlas glioma mri collections with expert segmentation labels and radiomic features. *Scientific data*, 4(1): 1–13, 2017. 6
- [12] Sophia Bano, Francisco Vasconcelos, Luke M Shepherd, Emmanuel Vander Poorten, Tom Vercauteren, Sebastien Ourselin, Anna L David, Jan Deprest, and Danail Stoyanov. Deep placental vessel segmentation for fetoscopic mosaicking. In *Medical Image Computing and Computer Assisted Intervention—MICCAI 2020: 23rd International Conference, Lima, Peru, October 4–8, 2020, Proceedings, Part III 23*, pages 763–773. Springer, 2020. 6
- [13] Rodrigo Benenson, Stefan Popov, and Vittorio Ferrari. Large-scale interactive object segmentation with human annotators. In *Proceedings of the IEEE/CVF conference on computer vision and pattern recognition*, pages 11700–11709, 2019. 2
- [14] Olivier Bernard, Alain Lalonde, Clement Zotti, Frederick Cervenansky, Xin Yang, Pheng-Ann Heng, Irem Cetin, Karim Lekadir, Oscar Camara, Miguel Angel Gonzalez Ballester, et al. Deep learning techniques for automatic mri cardiac multi-structures segmentation and diagnosis: is the problem solved? *IEEE transactions on medical imaging*, 37(11):2514–2525, 2018. 5, 6, 4, 7, 10
- [15] Patrick Bilic, Patrick Ferdinand Christ, Eugene Vorontsov, Grzegorz Chlebus, Hao Chen, Qi Dou, Chi-Wing Fu, Xiao Han, Pheng-Ann Heng, Jürgen Hesser, et al. The liver tumor segmentation benchmark (lits). *arXiv preprint arXiv:1901.04056*, 2019. 4, 6
- [16] Nicholas Bloch, Anant Madabhushi, Henkjan Huisman, John Freymann, Justin Kirby, Michael Grauer, Andinet Enquobahrie, Carl Jaffe, Larry Clarke, and Keyvan Farahani. Nci-isbi 2013 challenge: automated segmentation of prostate structures. *The Cancer Imaging Archive*, 370(6):5, 2015. 4, 6
- [17] Y.Y. Boykov and M.-P. Jolly. Interactive graph cuts for optimal boundary & region segmentation of objects in N-D images. In *Proceedings Eighth IEEE International Conference on Computer Vision. ICCV 2001*, pages 105–112, Vancouver, BC, Canada, 2001. IEEE Comput. Soc. 2
- [18] Gustav Bredell, Christine Tanner, and Ender Konukoglu. Iterative interaction training for segmentation editing networks. In *Machine Learning in Medical Imaging: 9th International Workshop, MLMI 2018, Held in Conjunction with MICCAI 2018, Granada, Spain, September 16, 2018, Proceedings 9*, pages 363–370. Springer, 2018. 2
- [19] Mateusz Buda, Ashirbani Saha, and Maciej A Mazurowski. Association of genomic subtypes of lower-grade gliomas with shape features automatically extracted by a deep learning algorithm. *Computers in biology and medicine*, 109: 218–225, 2019. 6
- [20] Victor Ion Butoi\*, Jose Javier Gonzalez Ortiz\*, Tianyu Ma, Mert R. Sabuncu, John Guttag, and Adrian V. Dalca. Universeg: Universal medical image segmentation. In *ICCV*, 2023. 2, 4, 3, 5
- [21] Juan C. Caicedo, Allen Goodman, Kyle W. Karhohs, Beth A. Cimini, Jeanelle Ackerman, Marzieh Haghighi, CherKeng Heng, Tim Becker, Minh Doan, Claire McQuin, Mohammad Rohban, Shantanu Singh, and Anne E. Carpenter. Nucleus segmentation across imaging experiments: the 2018 Data Science Bowl. *Nature Methods*, 16(12):1247–1253, 2019. 4, 6
- [22] Albert Cardona, Stephan Saalfeld, Stephan Preibisch, Benjamin Schmid, Anchi Cheng, Jim Pulokas, Pavel Tomancak, and Volker Hartenstein. An integrated micro-and macroarchitectural analysis of the drosophila brain by computer-assisted serial section electron microscopy. *PLoS biology*, 8(10):e1000502, 2010. 4, 6
- [23] Xi Chen, Yau Shing Jonathan Cheung, Ser-Nam Lim, and Hengshuang Zhao. ScribbleSeg: Scribble-based Interactive Image Segmentation, 2023. arXiv:2303.11320 [cs]. 2, 3
- [24] Junlong Cheng, Jin Ye, Zhongying Deng, Jianpin Chen, Tianbin Li, Haoyu Wang, Yanzhou Su, Ziyang Huang, Jilong Chen, Lei Jiang, Hui Sun, Junjun He, Shaoting Zhang, Min Zhu, and Yu Qiao. SAM-Med2D, 2023. arXiv:2308.16184 [cs]. 2, 6
- [25] Noel C. F. Codella, David A. Gutman, M. Emre Celebi, Brian Helba, Michael A. Marchetti, Stephen W. Dusza, Aadi

- Kaloo, Konstantinos Liopyris, Nabin K. Mishra, Harald Kittler, and Allan Halpern. Skin lesion analysis toward melanoma detection: A challenge at the 2017 international symposium on biomedical imaging (isbi), hosted by the international skin imaging collaboration (ISIC). *CoRR*, abs/1710.05006, 2017. 4, 6
- [26] Antonio Criminisi, Toby Sharp, and Andrew Blake. GeoS: Geodesic Image Segmentation. In *Computer Vision – ECCV 2008*, pages 99–112. Springer Berlin Heidelberg, Berlin, Heidelberg, 2008. Series Title: Lecture Notes in Computer Science. 2
- [27] Steffen Czolbe and Adrian V Dalca. Neuralizer: General neuroimage analysis without re-training. In *Proceedings of the IEEE/CVF Conference on Computer Vision and Pattern Recognition*, pages 6217–6230, 2023. 2
- [28] Adrian V Dalca, John Guttag, and Mert R Sabuncu. Anatomical priors in convolutional networks for unsupervised biomedical segmentation. In *Proceedings of the IEEE Conference on Computer Vision and Pattern Recognition*, pages 9290–9299, 2018. 6
- [29] Adrian V Dalca, John Guttag, and Mert R Sabuncu. Anatomical priors in convolutional networks for unsupervised biomedical segmentation. In *Proceedings of the IEEE Conference on Computer Vision and Pattern Recognition*, pages 9290–9299, 2018. 5, 19
- [30] Etienne Decenciere, Guy Cazuguel, Xiwei Zhang, Guillaume Thibault, J-C Klein, Fernand Meyer, Beatriz Marcotegui, Gwénolé Quellec, Mathieu Lamard, Ronan Danno, et al. Teleophta: Machine learning and image processing methods for teleophthalmology. *Irbm*, 34(2):196–203, 2013. 6
- [31] Aysen Degerli, Morteza Zabihi, Serkan Kiranyaz, Tahir Hamid, Rashid Mazhar, Ridha Hamila, and Moncef Gabbouj. Early detection of myocardial infarction in low-quality echocardiography. *IEEE Access*, 9:34442–34453, 2021. 6
- [32] Lee R Dice. Measures of the amount of ecologic association between species. *Ecology*, 26(3):297–302, 1945. 4, 5, 6, 1
- [33] Pedro F Felzenszwalb and Daniel P Huttenlocher. Efficient graph-based image segmentation. *International journal of computer vision*, 59:167–181, 2004. 4, 3
- [34] Bruce Fischl. Freesurfer. *Neuroimage*, 62(2):774–781, 2012. 5, 19
- [35] Marco Forte, Brian Price, Scott Cohen, Ning Xu, and François Pitié. Getting to 99% Accuracy in Interactive Segmentation, 2020. arXiv:2003.07932 [cs]. 2
- [36] J Gamper, NA Koohbanani, K Benes, S Graham, M Jahani-far, SA Khurram, A Azam, K Hewitt, and N Rajpoot. Pan-nuke dataset extension, insights and baselines. arxiv. 2020 doi: 10.48550. ARXIV, 2003. 4, 6
- [37] Stephan Gerhard, Jan Funke, Julien Martel, Albert Cardona, and Richard Fetter. Segmented anisotropic ssTEM dataset of neural tissue. 2013. 4, 7
- [38] Randy L Gollub, Jody M Shoemaker, Margaret D King, Tonya White, Stefan Ehrlich, Scott R Sponheim, Vincent P Clark, Jessica A Turner, Bryon A Mueller, Vince Magnotta, et al. The mcic collection: a shared repository of multi-modal, multi-site brain image data from a clinical investigation of schizophrenia. *Neuroinformatics*, 11:367–388, 2013. 4, 6
- [39] Ioannis S Gousias, Daniel Rueckert, Rolf A Heckemann, Leigh E Dyet, James P Boardman, A David Edwards, and Alexander Hammers. Automatic segmentation of brain mris of 2-year-olds into 83 regions of interest. *Neuroimage*, 40(2):672–684, 2008. 6
- [40] Ioannis S Gousias, A David Edwards, Mary A Rutherford, Serena J Counsell, Jo V Hajnal, Daniel Rueckert, and Alexander Hammers. Magnetic resonance imaging of the newborn brain: manual segmentation of labelled atlases in term-born and preterm infants. *Neuroimage*, 62(3):1499–1509, 2012. 6
- [41] L. Grady. Random Walks for Image Segmentation. *IEEE Transactions on Pattern Analysis and Machine Intelligence*, 28(11):1768–1783, 2006. 2
- [42] Endre Grøvik, Darvin Yi, Michael Iv, Elizabeth Tong, Daniel Rubin, and Greg Zaharchuk. Deep learning enables automatic detection and segmentation of brain metastases on multisequence mri. *Journal of Magnetic Resonance Imaging*, 51(1):175–182, 2020. 6
- [43] Daniel Gut. X-ray images of the hip joints. 1, 2021. Publisher: Mendeley Data. 4, 5, 7, 20
- [44] Kaiming He, Xiangyu Zhang, Shaoqing Ren, and Jian Sun. Delving deep into rectifiers: Surpassing human-level performance on imagenet classification. In *Proceedings of the IEEE international conference on computer vision*, pages 1026–1034, 2015. 4
- [45] Sheng He, Rina Bao, Jingpeng Li, Jeffrey Stout, Atle Bjornerud, P. Ellen Grant, and Yangming Ou. Computer-vision benchmark segment-anything model (sam) in medical images: Accuracy in 12 datasets, 2023. 2
- [46] Nicholas Heller, Fabian Isensee, Klaus H Maier-Hein, Xiaoshuai Hou, Chunmei Xie, Fengyi Li, Yang Nan, Guangrui Mu, Zhiyong Lin, Miofei Han, et al. The state of the art in kidney and kidney tumor segmentation in contrast-enhanced ct imaging: Results of the kits19 challenge. *Medical Image Analysis*, page 101821, 2020. 4, 6
- [47] Moritz R Hernandez Petzsche, Ezequiel de la Rosa, Uta Hanning, Roland Wiest, Waldo Valenzuela, Mauricio Reyes, Maria Meyer, Sook-Lei Liew, Florian Kofler, Ivan Ezhov, et al. Isles 2022: A multi-center magnetic resonance imaging stroke lesion segmentation dataset. *Scientific data*, 9(1):762, 2022. 4, 6
- [48] Andrew Hoopes, Malte Hoffmann, Douglas N. Greve, Bruce Fischl, John Guttag, and Adrian V. Dalca. Learning the effect of registration hyperparameters with hypermorph. *Machine Learning for Biomedical Imaging*, 1:1–30, 2022. 6, 7
- [49] AD Hoover, Valentina Kouznetsova, and Michael Goldbaum. Locating blood vessels in retinal images by piecewise threshold probing of a matched filter response. *IEEE Transactions on Medical imaging*, 19(3):203–210, 2000. 4, 7
- [50] Xinrong Hu, Xiaowei Xu, and Yiyu Shi. How to efficiently adapt large segmentation model(sam) to medical images, 2023. 2
- [51] Yuhao Huang, Xin Yang, Lian Liu, Han Zhou, Ao Chang, Xinrui Zhou, Rusi Chen, Junxuan Yu, Jiongquan Chen,

- Chaoyu Chen, Haozhe Chi, Xindi Hu, Deng-Ping Fan, Fajin Dong, and Dong Ni. Segment anything model for medical images?, 2023. [2](#)
- [52] Daniel P Huttenlocher, Gregory A. Klanderman, and William J Rucklidge. Comparing images using the hausdorff distance. *IEEE Transactions on pattern analysis and machine intelligence*, 15(9):850–863, 1993. [6](#)
- [53] Humans in the Loop. Teeth segmentation dataset. [4, 7](#)
- [54] Sergey Ioffe and Christian Szegedy. Batch normalization: Accelerating deep network training by reducing internal covariate shift. In *International conference on machine learning*, pages 448–456. pmlr, 2015. [1](#)
- [55] Fabian Isensee, Paul F. Jaeger, Simon A. A. Kohl, Jens Petersen, and Klaus H. Maier-Hein. nnU-Net: a self-configuring method for deep learning-based biomedical image segmentation. *Nature Methods*, 18(2):203–211, 2021. [1, 4, 8](#)
- [56] Yuanfeng Ji, Haotian Bai, Jie Yang, Chongjian Ge, Ye Zhu, Ruimao Zhang, Zhen Li, Lingyan Zhang, Wanling Ma, Xi-ang Wan, et al. Amos: A large-scale abdominal multi-organ benchmark for versatile medical image segmentation. *arXiv preprint arXiv:2206.08023*, 2022. [4, 6](#)
- [57] Rashed Karim, R James Housden, Mayuragoban Balasubramian, Zhong Chen, Daniel Perry, Ayesha Uddin, Yosra Al-Beyatti, Ebrahim Palkhi, Prince Acheampong, Samantha Obom, et al. Evaluation of current algorithms for segmentation of scar tissue from late gadolinium enhancement cardiovascular magnetic resonance of the left atrium: an open-access grand challenge. *Journal of Cardiovascular Magnetic Resonance*, 15(1):1–17, 2013. [6](#)
- [58] Ali Emre Kavur, M. Alper Selver, Oğuz Dicle, Mustafa Barış, and N. Sinem Gezer. CHAOS - Combined (CT-MR) Healthy Abdominal Organ Segmentation Challenge Data, 2019. [6, 7](#)
- [59] A. Emre Kavur, N. Sinem Gezer, Mustafa Barış, Sinem Aslan, Pierre-Henri Conze, Vladimir Groza, Duc Duy Pham, Soumick Chatterjee, Philipp Ernst, Savaş Özkan, Bora Baydar, Dmitry Lachinov, Shuo Han, Josef Pauli, Fabian Isensee, Matthias Perkonig, Rachana Sathish, Ronnie Rajan, Deb-doot Sheet, Gurbandurdy Dovletov, Oliver Speck, Andreas Nürnberger, Klaus H. Maier-Hein, Gözde Bozdağ Akar, Gözde Ünal, Oğuz Dicle, and M. Alper Selver. CHAOS Challenge - combined (CT-MR) healthy abdominal organ segmentation. *Medical Image Analysis*, 69:101950, 2021. [4, 6, 7](#)
- [60] SeungKyu Kim, Hyun-Jic Oh, Seonghui Min, and Won-Ki Jeong. Evaluation and improvement of segment anything model for interactive histopathology image segmentation, 2023. [2](#)
- [61] Diederik P Kingma and Jimmy Ba. Adam: A method for stochastic optimization. *arXiv preprint arXiv:1412.6980*, 2014. [4](#)
- [62] Serkan Kiranyaz, Aysen Degerli, Tahir Hamid, Rashid Mazhar, Rayyan El Fadil Ahmed, Raya-an Abouhasera, Morteza Zabihi, Junaid Malik, Ridha Hamila, and Moncef Gabbouj. Left ventricular wall motion estimation by active polynomials for acute myocardial infarction detection. *IEEE Access*, 8:210301–210317, 2020. [6](#)
- [63] Alexander Kirillov, Eric Mintun, Nikhila Ravi, Hanzi Mao, Chloe Rolland, Laura Gustafson, Tete Xiao, Spencer Whitehead, Alexander C. Berg, Wan-Yen Lo, Piotr Dollár, and Ross Girshick. Segment anything. In *ICCV*, 2023. [2, 4, 6, 1, 3, 8, 11, 12](#)
- [64] Markus Krönke, Christine Eilers, Desislava Dimova, Melanie Köhler, Gabriel Buschner, Lilit Schweiger, Lemo-nia Konstantinidou, Marcus Makowski, James Nagarajah, Nassir Navab, et al. Tracked 3d ultrasound and deep neural network-based thyroid segmentation reduce interobserver variability in thyroid volumetry. *Plos one*, 17(7):e0268550, 2022. [4, 7](#)
- [65] Hugo J Kuijf, J Matthijs Biesbroek, Jeroen De Bresser, Rutger Heinen, Simon Andermatt, Mariana Bento, Matt Berseth, Mikhail Belyaev, M Jorge Cardoso, Adria Casamitjana, et al. Standardized assessment of automatic segmentation of white matter hyperintensities and results of the wmh segmentation challenge. *IEEE transactions on medical imaging*, 38(11):2556–2568, 2019. [4, 7](#)
- [66] Maria Kuklisova-Murgasova, Paul Aljabar, Latha Srinivasan, Serena J Counsell, Valentina Doria, Ahmed Serag, Ioannis S Gousias, James P Boardman, Mary A Rutherford, A David Edwards, et al. A dynamic 4d probabilistic atlas of the developing brain. *NeuroImage*, 54(4):2750–2763, 2011. [4, 6](#)
- [67] Zoé Lambert, Caroline Petitjean, Bernard Dubray, and Su Kuan. Segthor: segmentation of thoracic organs at risk in ct images. In *2020 Tenth International Conference on Image Processing Theory, Tools and Applications (IPTA)*, pages 1–6. IEEE, 2020. [4, 7](#)
- [68] Bennett Landman, Zhoubing Xu, J Igelsias, Martin Styner, T Langerak, and Arno Klein. Miccai multi-atlas labeling beyond the cranial vault—workshop and challenge. In *Proc. MICCAI Multi-Atlas Labeling Beyond Cranial Vault Workshop Challenge*, page 12, 2015. [4, 5, 6, 7](#)
- [69] Sarah Leclerc, Erik Smistad, Joao Pedrosa, Andreas Østvik, Frederic Cervenansky, Florian Espinosa, Torvald Espeland, Erik Andreas Rye Berg, Pierre-Marc Jodoin, Thomas Grenier, et al. Deep learning for segmentation using an open large-scale dataset in 2d echocardiography. *IEEE transactions on medical imaging*, 38(9):2198–2210, 2019. [6, 7](#)
- [70] Hyeonsoo Lee and Won-Ki Jeong. Scribble2label: Scribble-supervised cell segmentation via self-generating pseudo-labels with consistency. In *Medical Image Computing and Computer Assisted Intervention—MICCAI 2020: 23rd International Conference, Lima, Peru, October 4–8, 2020, Proceedings, Part I 23*, pages 14–23. Springer, 2020. [3](#)
- [71] Guillaume Lemaître, Robert Martí, Jordi Freixenet, Joan C Vilanova, Paul M Walker, and Fabrice Meriaudeau. Computer-aided detection and diagnosis for prostate cancer based on mono and multi-parametric mri: a review. *Computers in biology and medicine*, 60:8–31, 2015. [4, 6](#)
- [72] Mingchao Li, Yuhan Zhang, Zexuan Ji, Keren Xie, Songtao Yuan, Qinghuai Liu, and Qiang Chen. Ipn-v2 and octa-500: Methodology and dataset for retinal image segmentation. *arXiv preprint arXiv:2012.07261*, 2020. [4, 6, 7](#)
- [73] Di Lin, Jifeng Dai, Jiaya Jia, Kaiming He, and Jian Sun. Scribblesup: Scribble-supervised convolutional networks for

- semantic segmentation. In *Proceedings of the IEEE conference on computer vision and pattern recognition*, pages 3159–3167, 2016. 3
- [74] Tsung-Yi Lin, Priya Goyal, Ross Girshick, Kaiming He, and Piotr Dollár. Focal loss for dense object detection. In *Proceedings of the IEEE international conference on computer vision*, pages 2980–2988, 2017. 4, 1
- [75] Xian Lin, Yangyang Xiang, Li Zhang, Xin Yang, Zengqiang Yan, and Li Yu. Samus: Adapting segment anything model for clinically-friendly and generalizable ultrasound image segmentation, 2023. 2
- [76] Geert Litjens, Robert Toth, Wendy van de Ven, Caroline Hoeks, Sjoerd Kerkstra, Bram van Ginneken, Graham Vincent, Gwenael Guillard, Neil Birbeck, Jindang Zhang, et al. Evaluation of prostate segmentation algorithms for mri: the promise12 challenge. *Medical image analysis*, 18(2):359–373, 2014. 4, 6
- [77] Qin Liu, Zhenlin Xu, Yining Jiao, and Marc Niethammer. iSegFormer: Interactive Segmentation via Transformers with Application to 3D Knee MR Images. In *Medical Image Computing and Computer Assisted Intervention (MICCAI)*, 2022. 2
- [78] Qin Liu, Zhenlin Xu, Gedas Bertasius, and Marc Niethammer. Simpleclick: Interactive image segmentation with simple vision transformers. In *Proceedings of the IEEE/CVF International Conference on Computer Vision*, pages 22290–22300, 2023. 2
- [79] Vebjorn Ljosa, Katherine L Sokolnicki, and Anne E Carpenter. Annotated high-throughput microscopy image sets for validation. *Nature methods*, 9(7):637–637, 2012. 4, 6
- [80] Maximilian T Löffler, Anjany Sekuboyina, Alina Jacob, Anna-Lena Grau, Andreas Scharr, Malek El Hussein, Mareike Kallweit, Claus Zimmer, Thomas Baum, and Jan S Kirschke. A vertebral segmentation dataset with fracture grading. *Radiology: Artificial Intelligence*, 2(4):e190138, 2020. 4, 7
- [81] Xiangde Luo, Wenjun Liao, Jianghong Xiao, Tao Song, Xiaofan Zhang, Kang Li, Guotai Wang, and Shaoting Zhang. Word: Revisiting organs segmentation in the whole abdominal region. *arXiv preprint arXiv:2111.02403*, 2021. 4, 7
- [82] Xiangde Luo, Guotai Wang, Tao Song, Jingyang Zhang, Michael Aertsen, Jan Deprest, Sebastien Ourselin, Tom Vercauteren, and Shaoting Zhang. MIDeepSeg: Minimally Interactive Segmentation of Unseen Objects from Medical Images Using Deep Learning. *Medical Image Analysis*, 72:102102, 2021. 1, 2, 6, 8
- [83] Jun Ma, Yao Zhang, Song Gu, Xingle An, Zhihe Wang, Cheng Ge, Congcong Wang, Fan Zhang, Yu Wang, Yinan Xu, et al. Fast and low-gpu-memory abdomen ct organ segmentation: the flare challenge. *Medical Image Analysis*, 82:102616, 2022. 6
- [84] Jun Ma, Yuting He, Feifei Li, Lin Han, Chenyu You, and Bo Wang. Segment anything in medical images. *Nature Communications*, 15:1–9, 2024. 2, 6, 4, 8
- [85] Yuhui Ma, Huaying Hao, Jianyang Xie, Huazhu Fu, Jiong Zhang, Jianlong Yang, Zhen Wang, Jiang Liu, Yalin Zheng, and Yitian Zhao. Rose: a retinal oct-angiography vessel segmentation dataset and new model. *IEEE Transactions on Medical Imaging*, 40(3):928–939, 2021. 4, 6
- [86] Jacob A. Macdonald, Zhe Zhu, Brandon Konkel, Maciej Mazurowski, Walter Wiggins, and Mustafa Bashir. Duke liver dataset (MRI) v2, 2023. 4
- [87] Kevis-Kokitsi Maninis, Sergi Caelles, Jordi Pont-Tuset, and Luc Van Gool. Deep Extreme Cut: From Extreme Points to Object Segmentation, 2018. arXiv:1711.09081. 2
- [88] Daniel S Marcus, Tracy H Wang, Jamie Parker, John G Csernansky, John C Morris, and Randy L Buckner. Open access series of imaging studies (oasis): cross-sectional mri data in young, middle aged, nondemented, and demented older adults. *Journal of cognitive neuroscience*, 19(9):1498–1507, 2007. 4, 6, 7
- [89] Kenneth Marek, Danna Jennings, Shirley Lasch, Andrew Siderowf, Caroline Tanner, Tanya Simuni, Chris Coffey, Karl Kieburtz, Emily Flagg, Sohini Chowdhury, et al. The parkinson progression marker initiative (ppmi). *Progress in neurobiology*, 95(4):629–635, 2011. 4, 6
- [90] Francesco Marzola, Nens Van Alfen, Jonne Doorduyn, and Kristen M. Meiburger. Deep learning segmentation of transverse musculoskeletal ultrasound images for neuromuscular disease assessment. *Computers in Biology and Medicine*, 135:104623, 2021. 6
- [91] Maciej A Mazurowski, Kal Clark, Nicholas M Czarnek, Parisa Shamsesfandabadi, Katherine B Peters, and Ashirbani Saha. Radiogenomics of lower-grade glioma: algorithmically-assessed tumor shape is associated with tumor genomic subtypes and patient outcomes in a multi-institutional study with the cancer genome atlas data. *Journal of neuro-oncology*, 133:27–35, 2017. 4, 6
- [92] Maciej A. Mazurowski, Haoyu Dong, Hanxue Gu, Jichen Yang, Nicholas Konz, and Yixin Zhang. Segment anything model for medical image analysis: An experimental study. *Medical Image Analysis*, 89:102918, 2023. 2
- [93] Jing Men, Yongyang Huang, Jitendra Solanki, Xianxu Zeng, Aneesh Alex, Jason Jerwick, Zhan Zhang, Rudolph E Tanzi, Airong Li, and Chao Zhou. Optical coherence tomography for brain imaging and developmental biology. *IEEE Journal of Selected Topics in Quantum Electronics*, 22(4):120–132, 2015. 1
- [94] Bjoern Menze, Leo Joskowicz, Spyridon Bakas, Andras Jakab, Ender Konukoglu, Anton Becker, Amber Simpson, and Richard D. Quantification of uncertainties in biomedical image quantification 2021. *4th International Conference on Medical Image Computing and Computer Assisted Intervention (MICCAI 2021)*, 2021. 6
- [95] Bjoern H Menze, Andras Jakab, Stefan Bauer, Jayashree Kalpathy-Cramer, Keyvan Farahani, Justin Kirby, Yuliya Burren, Nicole Porz, Johannes Slotboom, Roland Wiest, et al. The multimodal brain tumor image segmentation benchmark (brats). *IEEE transactions on medical imaging*, 34(10):1993–2024, 2014. 6
- [96] Fausto Milletari, Nassir Navab, and Seyed-Ahmad Ahmadi. V-net: Fully convolutional neural networks for volumetric medical image segmentation. *Fourth International Conference on 3D Vision (3DV)*, pages 565–571, 2016. 1

- [97] Anna Montoya, Hasnin, kaggle446, shirzad, Will Cukierski, and yffud. Ultrasound nerve segmentation, 2016. 4, 6
- [98] Alexander Ze Hwan Ooi, Zunaina Embong, Aini Ismafairus Abd Hamid, Rafidah Zainon, Shir Li Wang, Theam Foo Ng, Rostam Affendi Hamzah, Soo Siang Teoh, and Haidi Ibrahim. Interactive Blood Vessel Segmentation from Retinal Fundus Image Based on Canny Edge Detector. *Sensors*, 21(19):6380, 2021. 2
- [99] Jay N Paranjape, Nithin Gopalakrishnan Nair, Shameema Sikder, S Swaroop Vedula, and Vishal M Patel. Adaptivesam: Towards efficient tuning of sam for surgical scene segmentation. *arXiv preprint arXiv:2308.03726*, 2023. 2
- [100] Kelly Payette, Priscille de Dumast, Hamza Kebiri, Ivan Ezhov, Johannes C Paetzold, Suprosanna Shit, Asim Iqbal, Romesa Khan, Raimund Kottke, Patrice Grehten, et al. An automatic multi-tissue human fetal brain segmentation benchmark using the fetal tissue annotation dataset. *Scientific Data*, 8(1):1–14, 2021. 6
- [101] Lina Pedraza, Carlos Vargas, Fabián Narváez, Oscar Durán, Emma Muñoz, and Eduardo Romero. An open access thyroid ultrasound image database. In *10th international symposium on medical information processing and analysis*, page 92870W. SPIE / International Society for Optics and Photonics, 2015. 4, 6
- [102] Kenneth A Philbrick, Alexander D Weston, Zeynettin Akkus, Timothy L Kline, Panagiotis Korfiatis, Tomas Sakinis, Petro Kostandy, Arunnit Boonrod, Atefeh Zeinoddini, Naoki Takahashi, et al. Ril-contour: a medical imaging dataset annotation tool for and with deep learning. *Journal of digital imaging*, 32:571–581, 2019. 1, 2
- [103] Gašper Podobnik, Primož Strojjan, Primož Peterlin, Bulat Ibragimov, and Tomaž Vrtovec. HaN-Seg: The head and neck organ-at-risk CT and MR segmentation dataset. *Medical Physics*, 50(3):1917–1927, 2023. <https://aapm.onlinelibrary.wiley.com/doi/pdf/10.1002/mp.16197>. 4, 6
- [104] Prasanna Porwal, Samiksha Pachade, Ravi Kamble, Manesh Kokare, Girish Deshmukh, Vivek Sahasrabudhe, and Fabrice Meriaudeau. Indian diabetic retinopathy image dataset (idrid), 2018. 4, 6
- [105] Perry Radau, Yingli Lu, Kim Connelly, Gideon Paul, AJWG Dick, and Graham Wright. Evaluation framework for algorithms segmenting short axis cardiac mri. *The MIDAS Journal-Cardiac MR Left Ventricle Segmentation Challenge*, 49, 2009. 4, 5, 7, 13
- [106] Alec Radford, Jong Wook Kim, Chris Hallacy, Aditya Ramesh, Gabriel Goh, Sandhini Agarwal, Girish Sastry, Amanda Askell, Pamela Mishkin, Jack Clark, et al. Learning transferable visual models from natural language supervision. In *International conference on machine learning*, pages 8748–8763. PMLR, 2021. 2
- [107] Maithra Raghu, Chiyuan Zhang, Jon Kleinberg, and Samy Bengio. Transfusion: Understanding transfer learning for medical imaging. *Advances in neural information processing systems*, 32, 2019. 2
- [108] Martin Rajchl, Matthew C. H. Lee, Ozan Oktay, Konstantinos Kamnitsas, Jonathan Passerat-Palmbach, Wenjia Bai, Mellisa Damodaram, Mary A. Rutherford, Joseph V. Hajnal, Bernhard Kainz, and Daniel Rueckert. DeepCut: Object Segmentation From Bounding Box Annotations Using Convolutional Neural Networks. *IEEE Transactions on Medical Imaging*, 36(2):674–683, 2017. 2
- [109] Marianne Rakic, Hallee E Wong, Jose Javier Gonzalez Ortiz, Beth Cimini, John Guttag, and Adrian V Dalca. Tyche: Stochastic in-context learning for medical image segmentation. *arXiv preprint arXiv:2401.13650*, 2024. 4, 3
- [110] Blaine Rister, Darvin Yi, Kaushik Shivakumar, Tomomi Nobashi, and Daniel L. Rubin. CT-ORG, a new dataset for multiple organ segmentation in computed tomography. *Scientific Data*, 7(1):381, 2020. 4, 6
- [111] Olaf Ronneberger, Philipp Fischer, and Thomas Brox. U-net: Convolutional networks for biomedical image segmentation. In *Medical Image Computing and Computer-Assisted Intervention—MICCAI 2015: 18th International Conference, Munich, Germany, October 5–9, 2015, Proceedings, Part III 18*, pages 234–241. Springer, 2015. 1, 4
- [112] Holger R. Roth, Dong Yang, Ziyue Xu, Xiaosong Wang, and Daguang Xu. Going to Extremes: Weakly Supervised Medical Image Segmentation. *Machine Learning and Knowledge Extraction*, 3(2):507–524, 2021. 2
- [113] Carsten Rother, Vladimir Kolmogorov, and Andrew Blake. “GrabCut” — Interactive Foreground Extraction using Iterated Graph Cuts. *ACM Transactions on Graphics*, 23: 309–314, 2004. 2
- [114] Tomas Sakinis, Fausto Milletari, Holger Roth, Panagiotis Korfiatis, Petro Kostandy, Kenneth Philbrick, Zeynettin Akkus, Ziyue Xu, Daguang Xu, and Bradley J. Erickson. Interactive segmentation of medical images through fully convolutional neural networks, 2019. [arXiv:1903.08205](https://arxiv.org/abs/1903.08205). 1, 2
- [115] Adriel Saporta, Xiaotong Gui, Ashwin Agrawal, Anuj Pareek, SQ Truong, CD Nguyen, Van-Doan Ngo, Jayne Seekins, Francis G Blankenberg, AY Ng, et al. Deep learning saliency maps do not accurately highlight diagnostically relevant regions for medical image interpretation. *MedRxiv*, 2021. 4, 6
- [116] Pascal Sati, Ilena C George, Colin D Shea, María I Gaitán, and Daniel S Reich. Flair\*: a combined mr contrast technique for visualizing white matter lesions and parenchymal veins. *Radiology*, 265(3):926–932, 2012. 1
- [117] Constantin Seibold, Simon Reiß, Saquib Sarfraz, Matthias A. Fink, Victoria Mayer, Jan Sellner, Moon Sung Kim, Klaus H. Maier-Hein, Jens Kleesiek, and Rainer Stiefelhagen. Detailed annotations of chest x-rays via ct projection for report understanding. In *Proceedings of the 33th British Machine Vision Conference (BMVC)*, 2022. 4, 6, 7
- [118] Ahmed Serag, Paul Aljabar, Gareth Ball, Serena J Counsell, James P Boardman, Mary A Rutherford, A David Edwards, Joseph V Hajnal, and Daniel Rueckert. Construction of a consistent high-definition spatio-temporal atlas of the developing brain using adaptive kernel regression. *Neuroimage*, 59(3):2255–2265, 2012. 6
- [119] Arnaud Arindra Adiyoso Setio, Alberto Traverso, Thomas De Bel, Moira SN Berens, Cas Van Den Bogaard, Piergiorgio Cerello, Hao Chen, Qi Dou, Maria Evelina Fantacci,

- Bram Geurts, et al. Validation, comparison, and combination of algorithms for automatic detection of pulmonary nodules in computed tomography images: the luna16 challenge. *Medical image analysis*, 42:1–13, 2017. 4, 6
- [120] Peilun Shi, Jianing Qiu, Sai Mu Dalike Abaxi, Hao Wei, Frank P-W Lo, and Wu Yuan. Generalist vision foundation models for medical imaging: A case study of segment anything model on zero-shot medical segmentation. *Diagnostics*, 13(11):1947, 2023. 2
- [121] Amber L Simpson, Michela Antonelli, Spyridon Bakas, Michel Bilello, Keyvan Farahani, Bram Van Ginneken, Annette Kopp-Schneider, Bennett A Landman, Geert Litjens, Bjoern Menze, et al. A large annotated medical image dataset for the development and evaluation of segmentation algorithms. *arXiv preprint arXiv:1902.09063*, 2019. 4, 6
- [122] Konstantin Sofiiuk, Iliia Petrov, Olga Barinova, and Anton Konushin. F-BRS: Rethinking Backpropagating Refinement for Interactive Segmentation. In *2020 IEEE/CVF Conference on Computer Vision and Pattern Recognition (CVPR)*, pages 8620–8629, Seattle, WA, USA, 2020. IEEE. 2
- [123] Konstantin Sofiiuk, Iliia A. Petrov, and Anton Konushin. Reviving Iterative Training with Mask Guidance for Interactive Segmentation, 2021. *arXiv:2102.06583 [cs]*. 2, 4
- [124] Yuxin Song, Jing Zheng, Long Lei, Zhipeng Ni, Baoliang Zhao, and Ying Hu. CT2US: Cross-modal transfer learning for kidney segmentation in ultrasound images with synthesized data. *Ultrasonics*, 122:106706, 2022. 4, 6
- [125] Joes Staal, Michael D Abràmoff, Meindert Niemeijer, Max A Viergever, and Bram Van Ginneken. Ridge-based vessel segmentation in color images of the retina. *IEEE transactions on medical imaging*, 23(4):501–509, 2004. 4, 5, 18
- [126] Yucheng Tang, Dong Yang, Wenqi Li, Holger R. Roth, Bennett Landman, Daguang Xu, Vishwesh Nath, and Ali Hatamizadeh. Self-Supervised Pre-Training of Swin Transformers for 3D Medical Image Analysis. In *2022 IEEE/CVF Conference on Computer Vision and Pattern Recognition (CVPR)*, pages 20698–20708, New Orleans, LA, USA, 2022. IEEE. 1
- [127] Dmitry Ulyanov, Andrea Vedaldi, and Victor Lempitsky. Instance normalization: The missing ingredient for fast stylization. *arXiv preprint arXiv:1607.08022*, 2016. 1
- [128] Bram van Ginneken, Mikkel B. Stegmann, and Marco Loog. Segmentation of anatomical structures in chest radiographs using supervised methods: a comparative study on a public database. *Medical Image Analysis*, 10(1):19–40, 2006. 5, 14
- [129] Vladimir Vezhnevets and Vadim Konouchine. “GrowCut” - Interactive Multi-Label N-D Image Segmentation By Cellular Automata. *proc. of Graphicon*, 1(4):150–156, 2005. 2
- [130] Santiago Vitale, José Ignacio Orlando, Emmanuel Iarussi, and Ignacio Larrabide. Improving realism in patient-specific abdominal ultrasound simulation using cyclegans. *International journal of computer assisted radiology and surgery*, 15(2):183–192, 2020. 6, 7
- [131] Chengliang Wang, Xinrun Chen, Haojian Ning, and Shiyang Li. Sam-octa: A fine-tuning strategy for applying foundation model to octa image segmentation tasks, 2023. 2
- [132] Guotai Wang, Maria A. Zuluaga, Rosalind Pratt, Michael Aertsen, Tom Doel, Maria Klusmann, Anna L. David, Jan Deprest, Tom Vercauteren, and Sébastien Ourselin. Slic-Seg: A minimally interactive segmentation of the placenta from sparse and motion-corrupted fetal MRI in multiple views. *Medical Image Analysis*, 34:137–147, 2016. 2
- [133] Guotai Wang, Wenqi Li, Maria A. Zuluaga, Rosalind Pratt, Premal A. Patel, Michael Aertsen, Tom Doel, Anna L. David, Jan Deprest, Sebastien Ourselin, and Tom Vercauteren. Interactive Medical Image Segmentation Using Deep Learning With Image-Specific Fine Tuning. *IEEE Transactions on Medical Imaging*, 37(7):1562–1573, 2018. 1, 2
- [134] Guotai Wang, Maria A. Zuluaga, Wenqi Li, Rosalind Pratt, Premal A. Patel, Michael Aertsen, Tom Doel, Anna L. David, Jan Deprest, Sebastien Ourselin, and Tom Vercauteren. DeepIGeoS: A Deep Interactive Geodesic Framework for Medical Image Segmentation. *IEEE Transactions on Pattern Analysis and Machine Intelligence*, 41(7):1559–1572, 2019. 1, 2, 3
- [135] Xinlong Wang, Wen Wang, Yue Cao, Chunhua Shen, and Tiejun Huang. Images speak in images: A generalist painter for in-context visual learning. *arXiv preprint arXiv:2212.02499*, 2022. 2
- [136] Xinlong Wang, Xiaosong Zhang, Yue Cao, Wen Wang, Chunhua Shen, and Tiejun Huang. SegGPT: Segmenting Everything In Context, 2023. *arXiv:2304.03284 [cs]*. 2
- [137] Jakob Wasserthal, Hanns-Christian Breit, Manfred T Meyer, Maurice Pradella, Daniel Hinck, Alexander W Sauter, Tobias Heye, Daniel T Boll, Joshy Cyriac, Shan Yang, et al. Totalsegmentator: Robust segmentation of 104 anatomic structures in ct images. *Radiology: Artificial Intelligence*, 5(5), 2023. 4, 5, 21
- [138] Junde Wu, Rao Fu, Huihui Fang, Yuanpei Liu, Zhaowei Wang, Yanwu Xu, Yueming Jin, and Tal Arbel. Medical SAM Adapter: Adapting Segment Anything Model for Medical Image Segmentation, 2023. *arXiv:2304.12620 [cs]*. 2
- [139] Yuxin Wu and Kaiming He. Group normalization. In *Proceedings of the European conference on computer vision (ECCV)*, pages 3–19, 2018. 1
- [140] Ning Xu, Brian Price, Scott Cohen, Jimei Yang, and Thomas Huang. Deep Interactive Object Selection. In *2016 IEEE Conference on Computer Vision and Pattern Recognition (CVPR)*, pages 373–381, Las Vegas, NV, USA, 2016. IEEE. 2, 4
- [141] Ning Xu, Brian Price, Scott Cohen, Jimei Yang, and Thomas Huang. Deep GrabCut for Object Selection. *arXiv*, 2017. *arXiv:1707.00243*. 2
- [142] Jin Ye, Junlong Cheng, Jianpin Chen, Zhongying Deng, Tianbin Li, Haoyu Wang, Yanzhou Su, Ziyang Huang, Jilong Chen, Lei Jiang, et al. Sa-med2d-20m dataset: Segment anything in 2d medical imaging with 20 million masks. *arXiv preprint arXiv:2311.11969*, 2023. 4
- [143] Paul A Yushkevich, Joseph Piven, Heather Cody Hazlett, Rachel Gimpel Smith, Sean Ho, James C Gee, and Guido Gerig. User-guided 3d active contour segmentation of anatomical structures: significantly improved efficiency and reliability. *Neuroimage*, 31(3):1116–1128, 2006. 1, 2

- [144] Jianxiong Zhang, Xuefeng Ding, Dasha Hu, and Yuming Jiang. Semantic segmentation of covid-19 lesions with a multiscale dilated convolutional network. *Scientific Reports*, 12(1):1847, 2022. [1](#)
- [145] Kaidong Zhang and Dong Liu. Customized segment anything model for medical image segmentation, 2023. [2](#)
- [146] Shiyin Zhang, Jun Hao Liew, Yunchao Wei, Shikui Wei, and Yao Zhao. Interactive Object Segmentation With Inside-Outside Guidance. In *2020 IEEE/CVF Conference on Computer Vision and Pattern Recognition (CVPR)*, pages 12231–12241. IEEE, 2020. [2](#)
- [147] T. Y. Zhang and C. Y. Suen. A fast parallel algorithm for thinning digital patterns. *Commun. ACM*, 27(3):236–239, 1984. [3](#), [2](#)
- [148] Yingtao Zhang, Min Xian, Heng-Da Cheng, Bryar Shareef, Jianrui Ding, Fei Xu, Kuan Huang, Boyu Zhang, Chunping Ning, and Ying Wang. Busis: A benchmark for breast ultrasound image segmentation. In *Healthcare*, page 729. MDPI, 2022. [4](#), [6](#)
- [149] Qi Zhao, Shuchang Lyu, Wenpei Bai, Linghan Cai, Binghao Liu, Meijing Wu, Xiubo Sang, Min Yang, and Lijiang Chen. A multi-modality ovarian tumor ultrasound image dataset for unsupervised cross-domain semantic segmentation. *CoRR*, abs/2207.06799, 2022. [4](#), [6](#)
- [150] Guoyan Zheng, Chengwen Chu, Daniel L Belavý, Bulat Ibragimov, Robert Korez, Tomaž Vrtovec, Hugo Hutt, Richard Everson, Judith Meakin, Isabel López Andrade, et al. Evaluation and comparison of 3d intervertebral disc localization and segmentation methods for 3d t2 mr data: A grand challenge. *Medical image analysis*, 35:327–344, 2017. [4](#), [5](#), [7](#)
- [151] Xin Zheng, Yong Wang, Guoyou Wang, and Jianguo Liu. Fast and robust segmentation of white blood cell images by self-supervised learning. *Micron*, 107:55–71, 2018. [4](#), [5](#), [7](#)
- [152] Tianfei Zhou, Liulei Li, Gustav Bredell, Jianwu Li, Jan Unkelbach, and Ender Konukoglu. Volumetric memory network for interactive medical image segmentation. *Medical Image Analysis*, 83:102599, 2023. [1](#), [3](#)
- [153] Xueyan Zou, Jianwei Yang, Hao Zhang, Feng Li, Linjie Li, Jianfeng Wang, Lijuan Wang, Jianfeng Gao, and Yong Jae Lee. Segment everything everywhere all at once. *Advances in Neural Information Processing Systems*, 36, 2024. [2](#)



# ScribblePrompt: Fast and Flexible Interactive Segmentation for Any Biomedical Image

## Appendix

### Table of Contents

Appendix **A**: Demo and Code  
Appendix **B**: ScribblePrompt Implementation  
Appendix **D**: Experimental Setup  
Appendix **C**: Data  
Appendix **E**: Evaluation with Manual Scribbles  
Appendix **F**: Evaluation with Simulated Interactions  
Appendix **G**: User Study  
Appendix **H**: Inference Runtime  
Appendix **I**: Ablations

### A. Demo and Code

An interactive demo, code, model weights, and the Med-Scribble dataset are available at

<https://scribbleprompt.csail.mit.edu>

### B. ScribblePrompt Implementation

#### B.1. Prompt Simulation

In this section, we provide illustrations of the prompt simulation process. Each of these click and scribble simulation algorithms can be applied to the ground truth label (or false negative error region) to simulate positive clicks/scribbles and to the background (or false positive error region) to simulate negative clicks/scribbles.

##### B.1.1 Scribbles

We simulate diverse and varied scribbles by first generating clean scribbles using one of three methods: (i) line scribbles, (ii) centerline scribbles or (iii) contour scribbles. Then, we break up and warp the scribbles to add more variability to account for human error.

**Line Scribbles.** Fig. 8 illustrates the process of simulating line scribbles.

**Centerline Scribbles.** Fig. 9 illustrates the process of simulating centerline scribbles.

**Contour Scribbles.** Fig. 10 illustrates the process of simulating contour scribbles.

##### B.1.2 Clicks

**Interior Border Region Clicks.** Fig. 11 illustrates the process for simulating interior border region clicks.

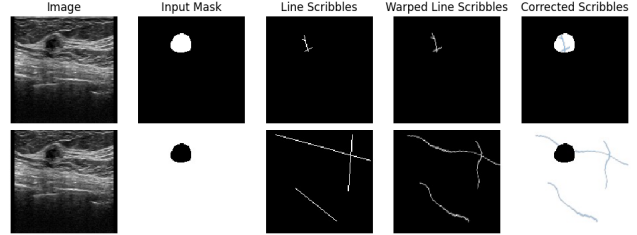


Figure 8. **Line scribbles.** Given an input mask  $z$ , we draw random lines by sampling two end points from  $\{(u, v) | z_{uv} = 1\}$ . We use a random deformation field to warp the line scribbles and then multiply by the binary input mask  $z$  to correct parts of the scribble that were warped outside the mask. We can simulate positive scribbles by applying the algorithm to the ground truth label  $y$  (top) and negative scribbles by applying the algorithm to the background  $1 - y$  (bottom).

#### B.2. Architecture and Training

We discuss some of the modeling decisions in ScribblePrompt-UNet and ScribblePrompt-SAM.

**Normalization Layers.** In preliminary experiments, we evaluated normalization layers in the ScribblePrompt-UNet architecture such as Batch Norm [54], Instance Norm [127], Layer Norm [8], and Channel Norm [139]. Including normalization did not improve the mean Dice on validation data compared to using no normalization layers (Fig. 12).

**Loss Function.** In preliminary experiments, we trained ScribblePrompt with Soft Dice Loss [32], a combination of Soft Dice Loss and Binary Cross-Entropy Loss, and a combination of Soft Dice Loss and Focal Loss [74], similar to [63]. In the latter two losses, Dice Loss and BCE Loss or Focal Loss are weighted equally. We found that the combination of Soft Dice Loss and Focal Loss resulted in slightly higher mean Dice on the validation data for ScribblePrompt-UNet and ScribblePrompt-SAM. Fig. 13 shows Dice recorded during training in preliminary experiments with ScribblePrompt-UNet.

**ScribblePrompt-UNet Inputs.** We encode each prompt type in an input channel for ScribblePrompt-UNet. The input to ScribblePrompt-UNet has size  $5 \times h \times w$  consisting of the input image  $x^t$ , bounding box encoding, positive click/scribble encoding, negative click/scribble encoding, and the logits of the previous prediction  $\hat{y}_{i-1}^t$ . For the first prediction, we set the previous prediction channel to zeros. We encode bounding boxes in a binary mask that is 1 inside the box(es) and

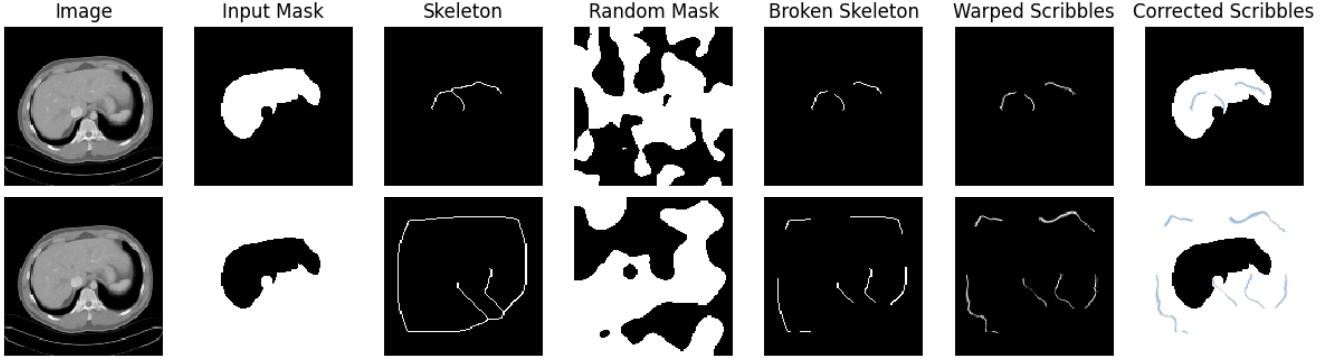


Figure 9. **Centerline scribbles.** Given an input mask, we apply a thinning algorithm [147] to get a 1-pixel wide skeleton. We break up the skeleton using a random mask and use a random deformation field to warp the broken skeleton. Lastly, we multiply the scribble mask by the input binary mask to remove parts of the scribble that were warped outside the input mask. We can simulate positive scribbles by applying the algorithm to the label  $y$  (top) and negative scribbles by applying the algorithm to the background  $1 - y$  (bottom).

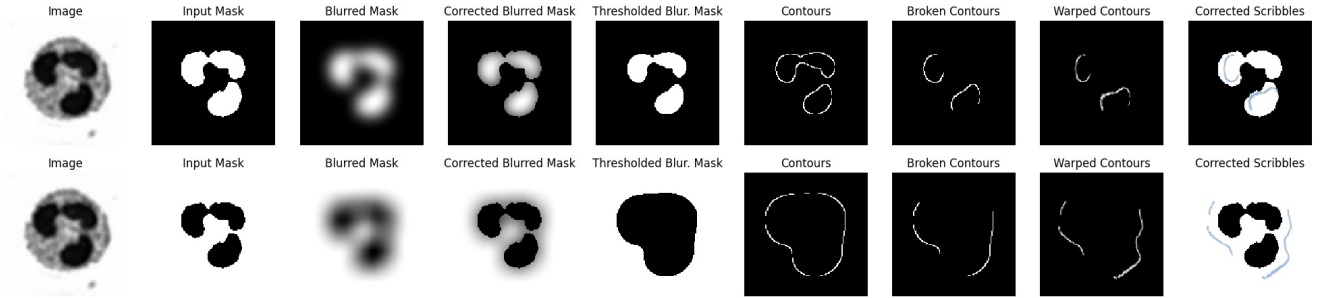


Figure 10. **Contour scribbles.** We simulate a rough contour of the desired segmentation within the boundaries of the label. Given a mask  $z$ , We first blur the mask to reduce the size of the label such that  $\tilde{z} = \min(z, z \circ G_k)$ , where  $G_k$  is a Gaussian blur kernel. Then we apply a threshold  $\tilde{z} < h$  sampled in some intensity range  $h \sim U[\tilde{z}_{min}, \tilde{z}_{max}]$  and extract a contour inside the boundary of the mask. We break up the contour using a random mask and use a random deformation field to warp the broken contour. Lastly, we multiply the scribble mask by the input binary mask to correct parts of the scribble that were warped outside the mask. We can simulate positive scribbles by applying the algorithm to the label  $y$  (bottom) and negative scribbles by applying the algorithm to the background  $1 - y$  (top).

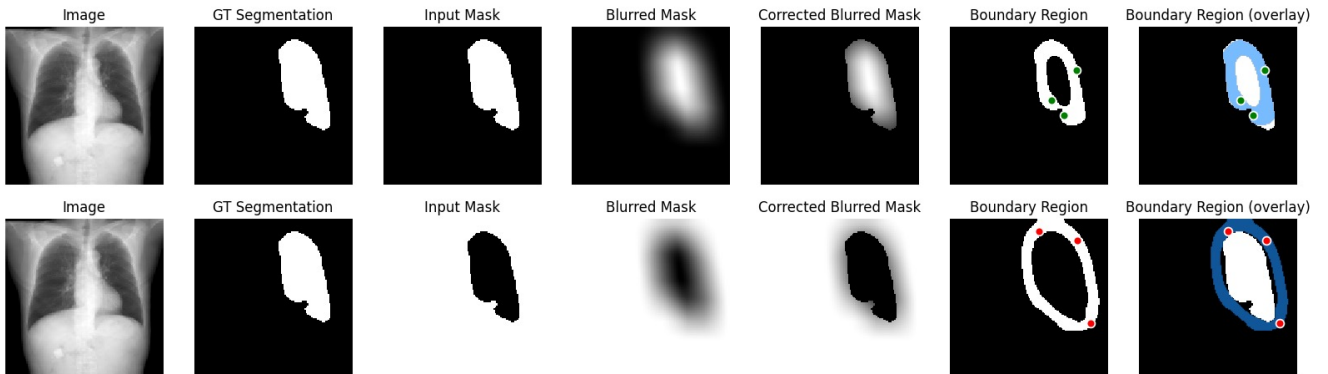


Figure 11. **Interior border region clicks.** We sample clicks from a border region inside the boundary of a given mask. Given a mask  $z$ , we first blur the mask to reduce the size of the label such that  $\tilde{z} = \min(z, z \circ G_k)$  where  $G_k$  is a Gaussian blur kernel. We then sample click coordinates from  $\{(u, v) | \tilde{z}_{uv} \in [a, b]\}$ , where  $a, b \sim U[\tilde{z}_{min}, \tilde{z}_{max}]$  are thresholds sampled in some intensity range. We show the simulation process for negative border region clicks on the background  $1 - y$  (top) and positive border region clicks on the label  $y$  (bottom).

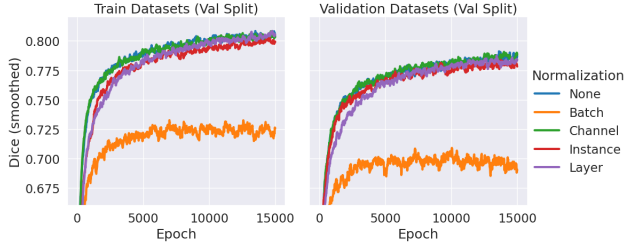


Figure 12. **Training ScribblePrompt-UNet with different normalization layers.** We show mean Dice averaged across five iterative predictions (using the training procedure for simulating interactions). At each epoch, we evaluate on 1,000 randomly sampled examples from the validation splits of the 65 training datasets and validation splits of the nine validation datasets. Dice was smoothed using Exponential Weighted Mean with  $\alpha = 0.1$ .

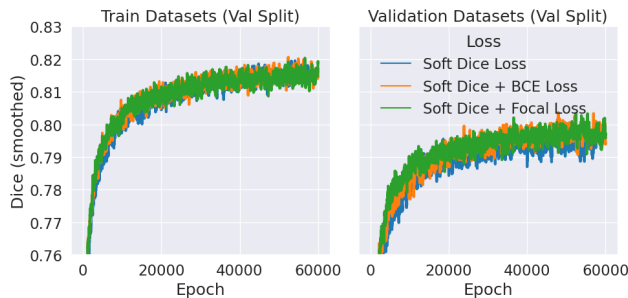


Figure 13. **Training ScribblePrompt-UNet with different loss functions.** We report Dice averaged across five iterative predictions (using the training procedure for simulating interactions). At each epoch, we evaluate on 1,000 randomly sampled examples from the validation splits of the 65 training datasets and validation splits of the nine validation datasets. Dice was smoothed using Exponential Weighted Mean with  $\alpha = 0.1$ .

0 everywhere else. We encode positive and negative clicks using binary masks where a pixel is 1 if has been clicked and 0 otherwise. We encode positive and negative scribbles as masks on  $[0, 1]$  and combine them with the masks encoding clicks. Representing the interactions as masks is advantageous because inference time does not scale with the number of interactions.

**ScribblePrompt-SAM Details.** To train ScribblePrompt-SAM, we took the pre-trained weights from SAM [63] with ViT-b backbone and froze all components of the network except for the decoder.

The SAM architecture can make predictions in single-mask mode or multi-mask mode. In *single-mask mode*, the decoder outputs a single predicted segmentation given an input image and user interactions. In *multi-mask mode*, the decoder predicts three possible segmentations and then outputs the segmentation with the highest predicted IoU by a MLP. We trained and evaluated ScribblePrompt-SAM in

multi-mask mode to maximize the expressiveness of the architecture. During training we included a MSE term in the segmentation loss to train the MLP to predict the IoU of the predictions, as in [63].

### B.3. Synthetic Labels

To help reduce task overfitting – memorizing the segmentation task for single-label datasets and thus ignoring user prompts – we introduce a mechanism to generate synthetic labels. During training, for a given sample  $(x_0, y_0)$ , with probability  $p_{synth}$  we replace  $y_0$  with a synthetic label  $y_{synth}$ .

We use a superpixel algorithm [33] with randomly sampled scale parameter  $\lambda \sim U[1, 500]$  to partition the image  $x_0$  into a map of  $k$  superpixels,  $z \in \{1, \dots, k\}^{n \times n}$ . Then, we randomly select a superpixel  $c \sim \text{Cat}(\{1, \dots, k\}, 1/k)$  as the synthetic label  $y_{synth} := \mathbb{1}[z = c]$ . Fig. 14 shows examples of training images and the corresponding maps of possible synthetic labels with different  $\lambda$ .

### C. Data

We build on large dataset gathering efforts like MegaMedical [20, 109] to compile a collection of 77 open-access biomedical imaging datasets for training and evaluation, covering over 54k scans, 16 image types, and 711 labels. We gathered datasets with a particular focus on Microscopy, X-Ray, and Ultrasound modalities, which were not as well represented in the original MegaMedical [20]. The full list of datasets is provided in Tab. 4, Tab. 5, and Tab. 6.

We define a 2D segmentation task as a combination of (sub)dataset, axis (for 3D modalities), and label. For datasets with multiple segmentation labels, we consider each label separately as a binary segmentation task. For datasets with sub-datasets (e.g., malignant vs. benign lesions) we consider each cohort as a separate task. For multi-annotator datasets, we treat each annotator as a separate label. For instance segmentation datasets, we sampled one instance at a time during training.

For 3D modalities we use the slice with maximum label area (“maxslice”) and the middle slice (“midslice”) for each volume for training of ScribblePrompt. We report results evaluating on maxslices, but we observed similar trends evaluating on midslices.

**Division of Datasets.** The division of datasets and subjects for training, model selection, and evaluation is summarized in Tab. 3. The 77 datasets were divided into 65 training datasets (Tables 5 and 6), 12 evaluation datasets. Data from 9 (out of 12) of the evaluation datasets was used in model development for model selection, and final evaluation. The other 3 evaluation datasets were completely held-out from model development and only used in the final evaluation.

**Division of Subjects.** We split each of the 77 datasets into 60% train, 20% validation, and 20% test by subject. We

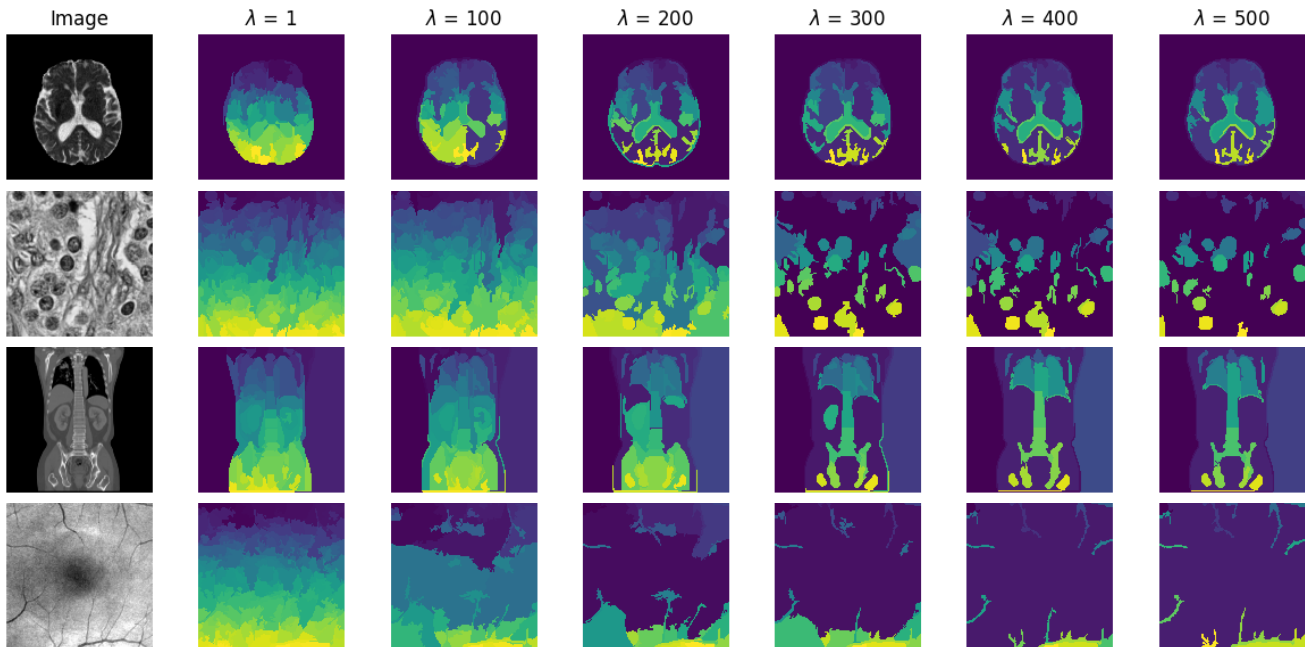


Figure 14. **Examples of possible synthetic labels.** Each color in the maps is a different synthetic label. During training, we replace a given label  $y_0$  with a synthetic label  $y_{synth}$  with probability  $p_{synth}$ . To generate  $y_{synth}$ , we apply a superpixel algorithm with randomly sampled scale parameter  $\lambda$  to the image  $x_0$  and then randomly select a superpixel as the synthetic label. We show examples of the synthetic label maps generated using a superpixel algorithm [33] with different  $\lambda$ .

used the “train” splits from the 65 training datasets to train ScribblePrompt models. We use the “validation” splits from the 65 training datasets and 9 validation datasets for model selection. We report final evaluation results across 12 evaluation sets consisting of the “test” splits of the 9 validation datasets *and* “test” splits of the 3 test datasets to maximize the diversity of tasks and modalities in our evaluation set (Tab. 3). No data from the 9 validation datasets or 3 test datasets were seen by ScribblePrompt models during training. For TotalSegmentator [137], we only evaluated on 20 examples per task due to the large number of tasks in the dataset. In total, the evaluation data cover 608 segmentation tasks.

**Image Processing.** We rescale image intensities to  $[0,1]$ . For methods using the SAM architecture, we convert the images to RGB and apply the pixel normalization scheme in [63].

**Image Resolution.** We resized images to  $128 \times 128$  for training of ScribblePrompt. We used this resolution to reduce training time during model development and to be able to conduct more thorough experiments. The ScribblePrompt approach is not tied to a particular resolution.

We conducted the experiments with MedScribble and simulated interactions with  $128^2$  size images. For the ACDC scribbles dataset and the user study we evaluated  $256^2$  size images to test ScribblePrompt’s performance at higher resolutions. Although the ScribblePrompt-UNet architecture can

take variable size inputs, we found downsizing the image to  $128^2$  for inference then upsampling the prediction to the input image size produced the highest Dice predictions.

For each method we resize the image to the method’s training image size before running inference. Although the SAM architecture takes input images of size  $1024^2$  (or  $256^2$  in the case of SAM-Med2D), the network outputs predictions of size  $256^2$  that are up-sampled to the input image size. MIDeepSeg takes  $96^2$  size images as inputs (after automatic cropping) and outputs predictions of size  $96^2$ .

**Interactive Baselines.** SAM-Med2D used three of our evaluation datasets (ACDC [14], BTCV [68] and TotalSegmentator [137]) as training datasets [142]. MedSAM used two of our evaluation datasets (TotalSegmentator [137] and BUID [5]) as training datasets [84].

**Supervised Baselines.** We trained fully-supervised baselines for 10 of our evaluation datasets. For those datasets, We used the train and validation splits to train a fully-supervised nnUNet [55] for each 2D task (Tab. 3). We report final results for all methods on the test splits of the evaluation datasets.

## D. Experimental Setup

**Training.** We use the Adam optimizer [61] and train with a learning rate of 0.0001 until convergence. We use a batch size of 8 for ScribblePrompt-UNet. For ScribblePrompt-

Table 3. **Dataset split overview.** Each dataset was split into 60% train, 20% validation and 20% test by subject. Data from the “train” splits of the 65 training datasets were used to train the models. The ScribblePrompt models did not see any data from the validation datasets or test datasets during training. Data from the “validation” split of the 9 validation datasets was used for ScribblePrompt ( SP ) model selection and baseline model selection (e.g., single-mask vs. multi-mask mode for SAM). We report final results on 12 “evaluation sets”: data from the “test” splits of the 9 validation datasets and the “test” splits of the 3 test datasets. To train the fully-supervised nnUNet baselines, we used the training and validation splits of the 12 evaluation datasets.

		Split within each dataset by subject		
Dataset Group	No. Datasets	Training Split (60%)	Validation Split (20%)	Test Split (20%)
Training Datasets	65	SP training	SP model selection	Not used
Validation Datasets	9	nnUNet training	SP and baselines model selection, nnUNet training	Final evaluation
Test Datasets	3	nnUNet training	nnUNet training	Final evaluation

Table 4. **Validation and test datasets.** We assembled the following set of datasets to evaluate ScribblePrompt and baseline methods. For the relative size of datasets, we include the number of unique scans (subject and modality pairs) that each dataset has. These datasets were unseen by ScribblePrompt during training. Three test datasets were completely held-out from model selection and development. The validation splits of the other 9 (validation) datasets were used for model selection. We report final results on the test splits of these 12 datasets.

Dataset Name	Description	Scans	Labels	Modalities
ACDC [14]	Left and right ventricular endocardium	99	3	cine-MRI
BTCV Cervix [68]	Bladder, uterus, rectum, small bowel	30	4	CT
BUID [5]	Breast tumors	647	2	Ultrasound
COBRE [4, 29, 34]	Brain anatomy	258	45	T1-weighted MRI
DRIVE [125]	Blood vessels in retinal images	20	1	Optical camera
HipXRray [43]	Ilium and femur	140	2	X-Ray
PanDental [1]	Mandible and teeth	215	2	X-Ray
SCD [105]	Sunnybrook Cardiac Multi-Dataset Collection	100	1	cine-MRI
SCR [128]	Lungs, heart, and clavicles	247	5	X-Ray
SpineWeb [150]	Vertebrae	15	1	T2-weighted MRI
TotalSegmentator [137]	104 anatomic structures (27 organs, 59 bones, 10 muscles, and 8 vessels)	1,204	104	CT
WBC [151]	White blood cell cytoplasm and nucleus	400	2	Microscopy

SAM we use a batch size of 1, because of memory constraints.

**Task Diversity.** The final ScribblePrompt-UNet and ScribblePrompt-SAM models were trained with  $p_{synth} = 0.5$ . Tab. 7 shows the data augmentations we used, similar to the in-task augmentations from [20].

**SAM Baselines.** For baseline methods using the SAM architecture, we evaluate the models in both “single mask” and “multi-mask” mode. For each baseline method and interaction procedure, we selected the best performing mode based on the average Dice across the validation data and report final results on test data using that mode. In the results with simulated clicks and scribbles by dataset in Appendix F.2, we show results using both modes. For ScribblePrompt-SAM and SAM-Med2D with adapter layers, multi-mask mode resulted in the highest Dice. For SAM-Med2D without adapter

layers, we found multi-mask mode led to higher Dice for scribble inputs while single-mask mode led to higher Dice with click inputs. For SAM (ViT-b and ViT-h) and MedSAM, single-mask mode resulted in the higher Dice on average.

## E. Manual Scribbles

We provide additional setup details and visualizations for the manual scribbles evaluation in Sec. 5.1.

### E.1. Setup

**MedScribble Dataset.** We collected a diverse dataset of manual scribble annotations, which is available at [scribbleprompt.csail.mit.edu](https://scribbleprompt.csail.mit.edu). The MedScribble dataset contains annotations from 3 annotators for 64 image-segmentation pairs. The examples were randomly selected from the validation split of 14 different datasets (7 training datasets and 7

Table 5. **Train datasets (part 1 of 2)**. We assembled the following set of datasets to train ScribblePrompt. For the relative size of datasets, we have included the number of unique scans (subject and modality pairs) that each dataset has.

Dataset Name	Description	Scans	Modalities
AbdominalUS [130]	Abdominal organ segmentation	1,543	Ultrasound
AMOS [56]	Abdominal organ segmentation	240	CT, MRI
BBBC003 [79]	Mouse embryos	15	Microscopy
BBBC038 [21]	Nuclei instance segmentation	670	Microscopy
BrainDev [39, 40, 66, 118]	Adult and neonatal brain atlases	53	Multimodal MRI
BrainMetShare[42]	Brain tumors	420	Multimodal MRI
BRATS [10, 11, 95]	Brain tumors	6,096	Multimodal MRI
BTCV Abdominal [68]	13 abdominal organs	30	CT
BUSIS [148]	Breast tumors	163	Ultrasound
CAMUS [69]	Four-chamber and Apical two-chamber heart	500	Ultrasound
CDemris [57]	Human left atrial wall	60	CMR
CHAOS [58, 59]	Abdominal organs (liver, kidneys, spleen)	40	CT, T2-weighted MRI
CheXplanation [115]	Chest X-Ray observations	170	X-Ray
CT2US [124]	Liver segmentation in synthetic ultrasound	4,586	Ultrasound
CT-ORG[110]	Abdominal organ segmentation (overlap with LiTS)	140	CT
DDTI [101]	Thyroid segmentation	472	Ultrasound
EOphtha [30]	Eye microaneurysms and diabetic retinopathy	102	Optical camera
FeTA [100]	Fetal brain structures	80	Fetal MRI
FetoPlac [12]	Placenta vessel	6	Fetoscopic optical camera
FLARE [83]	Abdominal organs (liver, kidney, spleen, pancreas)	361	CT
HaN-Seg [103]	Head and neck organs at risk	84	CT, T1-weighted MRI
HMC-QU [31, 62]	4-chamber (A4C) and apical 2-chamber (A2C) left wall	292	Ultrasound
I2CVB [71]	Prostate (peripheral zone, central gland)	19	T2-weighted MRI
IDRID [104]	Diabetic retinopathy	54	Optical camera
ISBI-EM [22]	Neuronal structures in electron microscopy	30	Microscopy
ISIC [25]	Dermoscopic lesions	2,000	Dermatology
ISLES [47]	Ischemic stroke lesion	180	Multimodal MRI
KiTS [46]	Kidney and kidney tumor	210	CT
LGGFlair [19, 91]	TCIA lower-grade glioma brain tumor	110	MRI
LiTS [15]	Liver tumor	131	CT
LUNA [119]	Lungs	888	CT
MCIC [38]	Multi-site brain regions of schizophrenic patients	390	T1-weighted MRI
MMOTU [149]	Ovarian tumors	1,140	Ultrasound
MSD [121]	Large-scale collection of 10 medical segmentation datasets	3,225	CT, Multimodal MRI
MuscleUS [90]	Muscle segmentation (biceps and lower leg)	8,169	Ultrasound
NCI-ISBI [16]	Prostate	30	T2-weighted MRI
NerveUS [97]	Nerve segmentation	5,635	Ultrasound
OASIS [48, 88]	Brain anatomy	414	T1-weighted MRI
OCTA500 [72]	Retinal vascular	500	OCT/OCTA
PanNuke [36]	Nuclei instance segmentation	7,901	Microscopy
PAXRay [117]	92 labels covering lungs, mediastinum, bones, and sub-diaphragm in Chest X-Ray	852	X-Ray
PROMISE12 [76]	Prostate	37	T2-weighted MRI
PPMI [28, 89]	Brain regions of Parkinson patients	1,130	T1-weighted MRI
QUBIQ [94]	Collection of 4 multi-annotator datasets (brain, kidney, pancreas and prostate)	209	T1-weighted MRI, Multimodal MRI, CT
ROSE [85]	Retinal vessel	117	OCT/OCTA

Table 6. **Train datasets (part 2 of 2)**. We assembled the following set of datasets to train ScribblePrompt. For the relative size of datasets, we have included the number of unique scans (subject and modality pairs) that each dataset has.

Dataset Name	Description	Scans	Modalities
SegTHOR [67]	Thoracic organs (heart, trachea, esophagus)	40	CT
SegThy [64]	Thyroid and neck segmentation	532	MRI, Ultrasound
ssTEM [37]	Neuron membranes, mitochondria, synapses and extracellular space	20	Microscopy
STARE [49]	Blood vessels in retinal images (multi-annotator)	20	Optical camera
ToothSeg [53]	Individual teeth	598	X-Ray
VerSe [80]	Individual vertebrae	55	CT
WMH [65]	White matter hyper-intensities	60	Multimodal MRI
WORD [81]	Abdominal organ segmentation	120	CT

Augmentation	$p$	Parameters
Random Affine	0.5	degrees $\in [0, 360]$ translation $\in [0, 0.2]$ scale $\in [0.8, 1.1]$
Brightness Contrast	0.5	brightness $\in [-0.1, 0.1]$ contrast $\in [0.8, 1.2]$
Gaussian Blur	0.5	$\sigma \in [0.1, 1.1]$ $k = 5$
Gaussian Noise	0.5	$\mu \in [0, 0.05]$ $\sigma \in [0, 0.05]$
Elastic Transform	0.25	$\alpha \in [1, 2]$ $\sigma \in [6, 8]$
Sharpness	0.5	sharpness = 5
Horizontal Flip	0.5	None
Vertical Flip	0.5	None

Table 7. **Data augmentations during training**. For each example, an augmentation is sampled with probability  $p$ . We apply augmentations after (optional) synthetic label generation and before simulating user interactions.

validation datasets) [1, 14, 43, 48, 49, 58, 59, 68, 69, 72, 88, 105, 117, 130, 150, 151].

For each task, the annotators were shown 5 training examples with the ground truth segmentation and instructed to draw positive scribbles on the region of interest and negative scribbles on the background for 3-5 new images (without seeing the ground truth segmentation). We collected the scribbles using a web app developed in Python using the Gradio library [2]. Two of the annotators used an iPad with stylus and one annotator used a laptop trackpad, to draw the scribbles.

For the manual scribbles evaluation, we report results on a subset of MedScribble, containing only examples from datasets unseen by ScribblePrompt during training. This subset contains 31 image-segmentation pairs (each with 3 sets annotations) covering 7 segmentations tasks from 7

different validation datasets [1, 14, 43, 68, 105, 150, 151]. The subset includes cardiac MRI, dental X-Ray, abdominal organ, spine vertebrae, and cell microscopy segmentation tasks.

**ACDC Scribbles Dataset.** Like the other datasets we used, we split the ACDC dataset [14] into 60% train, 20% validation and 20% test by subject. We used the validation split for model selection for baseline methods (e.g. single-mask vs. multi-mask mode for methods using the SAM architecture). We report results averaged across three labels on all slices for the test subjects.

**MedSAM.** We only evaluate MedSAM using bounding box prompts because it was fine-tuned exclusively with bounding box prompts and performs poorly with point inputs (Fig. 24). We prompted MedSAM using a bounding box fit to the positive scribbles. For each dataset, we experimented with using the minimum enclosing bounding box or enlarging the box by 5 pixels in each direction and selected the settings that maximized Dice on the validation data. Using the minimum bounding box resulted in higher Dice scores for MedScribble and enlarging the bounding box resulted in higher Dice scores for ACDC.

**SAM.** For methods using the SAM architecture (besides MedSAM), we converted the scribble masks to sets of positive and negative clicks for every non-zero pixel in the scribble masks.

**ScribblePrompt-UNet.** For ScribblePrompt-UNet we found that blurring the scribble masks with a 3x3 Gaussian blur kernel with  $\sigma = 0.5$  prior to inference improved Dice scores, perhaps due to differences in the distribution of pixel values between the manually-collected scribbles and simulated scribbles during training. We also experimented with blurring the scribbles for ScribblePrompt-SAM and each of the baseline methods but it did not improve the Dice scores for any other methods.

## E.2. Results

**Visualizations.** Fig. 15 shows predictions for each method using examples from the MedScribble dataset. Fig. 16 shows examples from the ACDC scribbles dataset.

## F. Simulated Interactions

We present additional results from experiments with simulated interactions (Sec. 5.2).

### F.1. Bounding Boxes

We evaluate models with simulated bounding box prompts.

**Setup.** We evaluate segmentation accuracy using Dice score after a single bounding box prompt. We simulate bounding boxes using the same procedure as used was used when training ScribblePrompt: we find the minimum enclosing bounding box for the ground truth label and then enlarge each dimension by  $r \sim U[0, 20]$  pixels to account for human error. We exclude MIDeepSeg [82] from this evaluation because it is not designed to make predictions from a single bounding box input.

For methods using the SAM architecture, we apply the pixel normalization scheme in [63] to images before inference. Upon further investigation, MedSAM [84] performed better with images rescaled to  $[0, 1]$ ; we report results for MedSAM with both normalization schemes.

**Results.** Fig. 17 shows mean Dice after one bounding box prompt. Fig. 18 shows results by dataset. ScribblePrompt-SAM has the highest Dice on average after one bounding box prompt.

**Visualizations.** Due the ambiguity of many segmentation tasks, its often difficult to predict an accurate segmentation from a single bounding box prompt (Fig. 20). Although ScribblePrompt models produced the highest dice predictions from a single bounding box prompt in Fig. 17, users may not be satisfied with this level of accuracy. Users can still achieve high Dice segmentations with ScribblePrompt by providing additional click and scribble interactions to correct the prediction. We visualize predictions for two examples in Fig. 19 and Fig. 20, after a single bounding box prompt and after correction clicks. MedSAM has the highest mean Dice among the baselines after a single bounding box prompt (Fig. 17), but its usability is limited because it cannot incorporate corrections.

### F.2. Scribbles and Clicks

We provide additional setup details, baselines and results for the experiments with simulated scribbles and clicks presented in Sec. 5.2.

**Setup.** We evaluated each method following three scribble interaction procedures and three click interaction procedures.

We provide details below on the MedSAM baseline and additional supervised baselines.

**MedSAM.** Since MedSAM [84] performs poorly with scribble and click prompts (Fig. 24), we only evaluate it with bounding box prompts. We fit a bounding box to the ground truth segmentation and enlarged each dimension by  $r \sim U[0, 10]$  pixels, to match the amount of jitter used during training for MedSAM. We show the mean Dice of segmentations predicted by MedSAM from a single bounding box prompt as a horizontal line (Fig. 21, Fig. 22) because MedSAM cannot incorporate corrections.

**Supervised Baselines.** We trained fully-supervised task-specific nnUNets [55] for 10 of the evaluation datasets. We show the mean Dice of the segmentations predicted by the ensemble of nnUNets using horizontal lines in the results by dataset (Fig. 29-34).

**Results.** Fig. 21 shows Dice vs. steps of interaction for three simulated click-focused procedures and three simulated scribble-focused procedures. On average, ScribblePrompt-UNet and ScribblePrompt-SAM have the highest Dice among interactive methods at all steps for all of the simulated interaction procedures. For select interaction procedures we also show HD95 vs. steps of interaction (Fig. 22). ScribblePrompt-UNet and ScribblePrompt-SAM consistently achieve the lowest HD95.

**Results by Dataset.** Figs. 29, 30, and 31 show quantitative results by dataset for the click-focused interaction procedures. Figs. 32, 33, and 34 show quantitative results by dataset for scribble-focused interaction procedures. ScribblePrompt reaches (or surpasses) fully-supervised nnUNet performance for 5 unseen datasets within 1-3 centerline scribbles steps, and for 10 unseen datasets within 6 scribble steps (Fig. 33).

**Visualizations.** We show predictions for test examples from evaluation datasets unseen by ScribblePrompt during training. Fig. 23, Fig. 25, and Fig. 26 show iterative predictions from each method using clicks. ScribblePrompt is able to segment large ambiguous objects (Fig. 23), as well as thin structures like vasculature (Fig. 25). For large and complex regions of interest such as white matter in brain MRI (Fig. 26), starting with a few random clicks at once is helpful.

Fig. 27 and Fig. 28 show iterative interactive segmentation with centerline scribbles and line scribbles. ScribblePrompt is able to accurately segment labels unseen during training using scribbles.

## G. User Study

We conducted a user study comparing ScribblePrompt-UNet to SAM (ViT-b). We provide additional details on the design and implementation of the user study.

**Study Design.** The goal of the user study was to compare



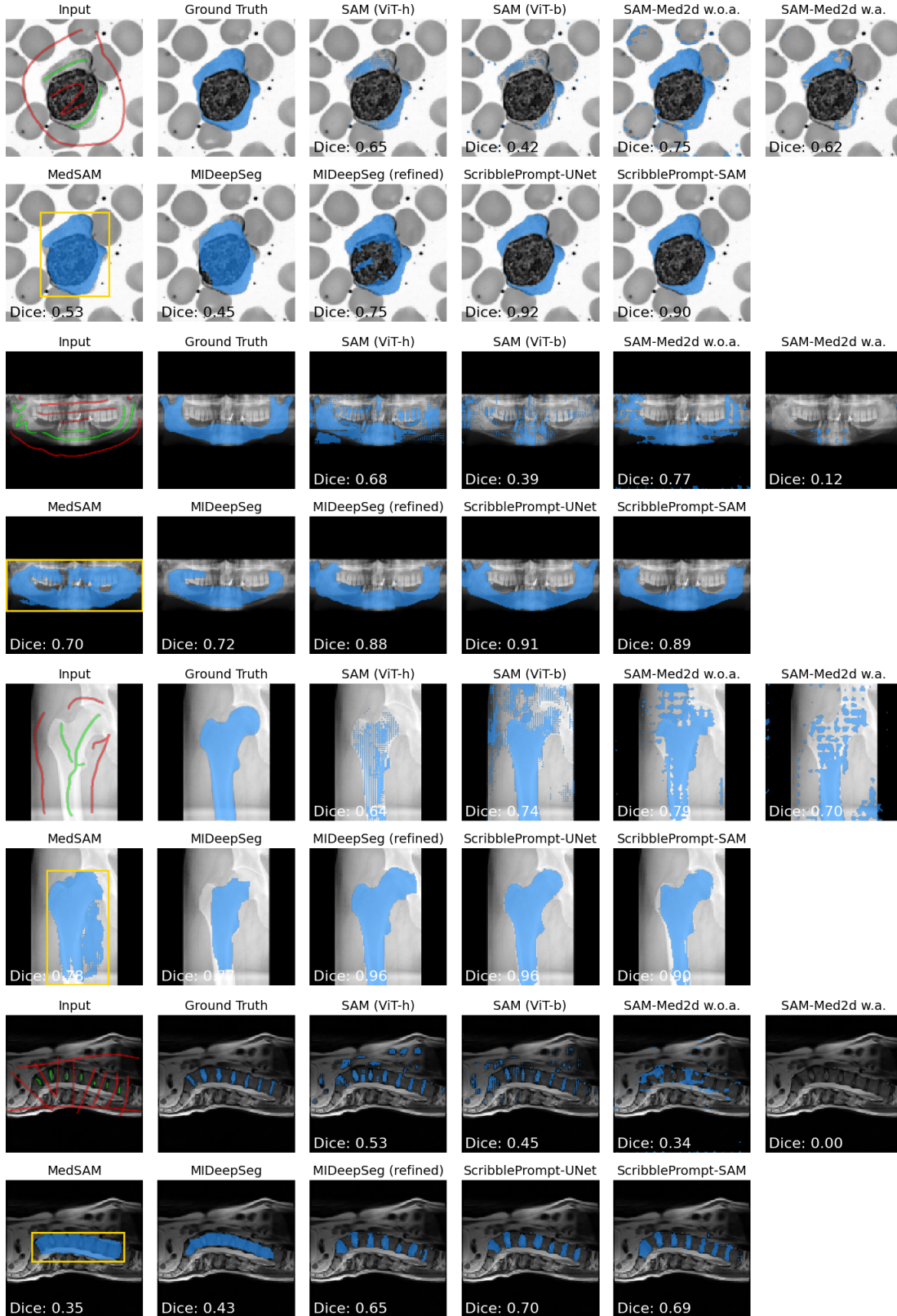


Figure 15. **Example predictions from MedScribble manual scribbles.** We evaluate on four examples from the MedScribble dataset. For each method, we show the **predicted segmentation** given a set of manually-collected **positive** and **negative** scribbles as input. For MedSAM, we use a bounding box fit to the positive scribbles as the input.

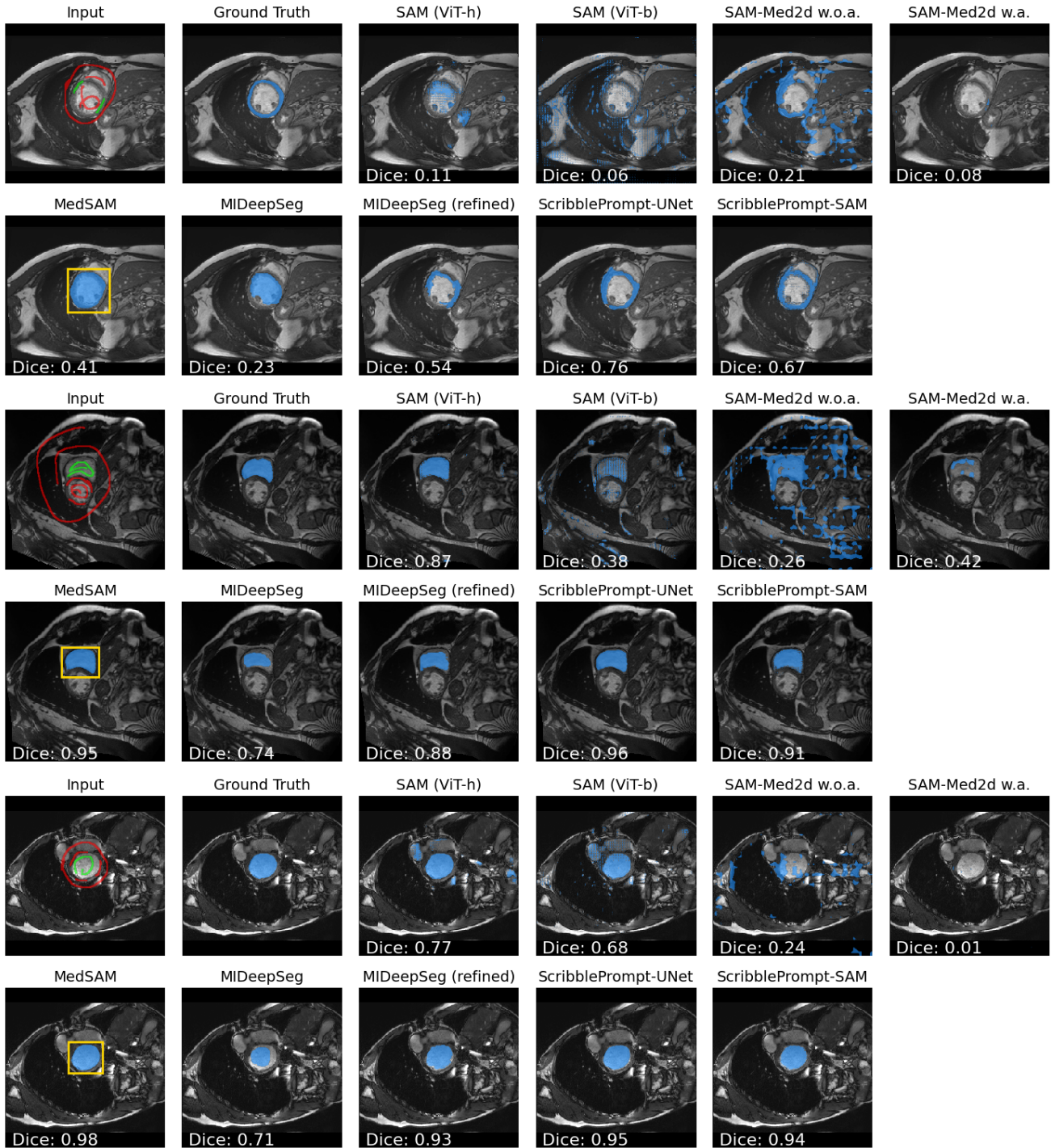


Figure 16. **Example predictions from ACDC manual scribbles.** We show examples for each label from the ACDC scribbles dataset [14]. For each method, we show the **predicted segmentation** given a set of manually-collected **positive** and **negative** scribbles as input. For MedSAM, we use a bounding box fit to the positive scribbles with 5 pixels added to each dimension as the input. Scribble thickness is enlarged for visual clarity.

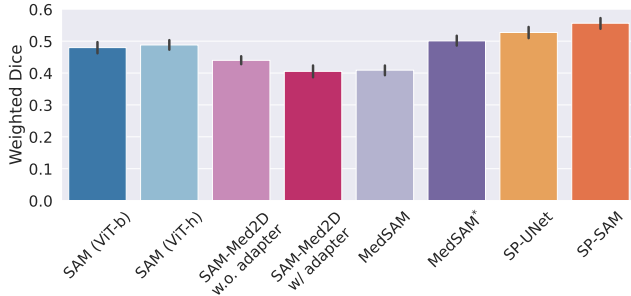


Figure 17. **Results with simulated bounding boxes.** Mean Dice on test data from 12 datasets with one simulated bounding box prompt, weighting each dataset equally. SP = ScribblePrompt. MedSAM\* indicates MedSAM with input images re-scaled to  $[0, 1]$  instead of the pixel normalization from [63]. Errorbars show 95% CI from bootstrapping.

ScribblePrompt to the best click-focused baseline method in terms of accuracy (Dice of the final segmentations), efficiency (time to achieve the desired segmentations) and user experience (perceived effort). Participants were given time to familiarize themselves with both models on a fixed set of practice images. Afterwards they used each model to segment a series of nine new test images from nine tasks that were not seen by the model during training (Fig. 35).

The order in which participants used the models, and which image the users were assigned to segment with each model for each task was randomized. We randomly selected one training image per task to include in the set of practice images. We randomly selected two test images per task and randomized the assignment of each image to each model for each participants. Each participant segmented a total of 18 images during the study. The models were also anonymized (i.e., “Model A” and “Model B”). We informed participants that one model was designed to be used with clicks and bounding boxes, while the other was designed for use with clicks, bounding boxes, and scribbles.

For each segmentation task, the participants were shown the target segmentation and were asked to interact with the model until the predicted segmentation closely matched the target or they could no longer improve the prediction. We provided participants with the target segmentation to disentangle the cognitive process of identifying the region of interest from prompting the model to achieve the desired segmentation.

**Study Participants.** Study participants were neuroimaging researchers at an academic hospital. Although the participants had prior experience with medical image segmentation, they did not necessarily have experience with the specific tasks and types of images used in the study.

We had a total of 29 participants with 16 participants completing all of the segmentations and the exit survey. We

observed a higher attrition rate among participants who were assigned to use SAM first, even after being able to freely try out both models during the “practice” phase. Among the 13 participants assigned to use SAM first, 62% did not finish all of their segmentations, compared with 31% among the 16 assigned to use ScribblePrompt first. We report results on the 16 participants who completed all the segmentations and the exit survey.

**Implementation.** Each participant used a web-based interface powered by a Nvidia Quatro RTX8000 GPU with 4 CPUs. Participants segmented the images at  $256 \times 256$  resolution. The interface was developed in Python using the Gradio library [2]. The interface had a “practice” mode in which users could freely switch between the two models and images from the set of practice images. After experimenting with both models, users clicked a button to begin “recorded activity” mode in which users were led through performing specific segmentation tasks with specific models. Users provided positive/negative scribble inputs, positive/negative click inputs and/or bounding box inputs, and then clicked a button to receive a prediction from the model.

**Survey Results.** Common factors that influenced participants preference for ScribblePrompt was being able to get accurate predictions from scribbles (“[ScribblePrompt] was more spatially smooth”), the model’s responsiveness to a variety of inputs (“it landed on my desired predictions more easily”), and less perceived effort when using the model (“[ScribblePrompt] needed much less guidance”). Participants preferred using clicks and bounding boxes over scribbles with SAM, praising its “snapiness”, the effectiveness of “exclusion clicks” and remarking it worked well for “rigid structures”. However, participants also noted in some cases “[SAM] did not respect object boundaries”, and for tasks such as retinal vein segmentation “[SAM] required lots of clicks and still was not very accurate”.

**Visualizations.** We visualize some of the interactions used by study participants and the resulting predictions in Fig. 35. Study participants used denser clicks when prompting SAM compared to when prompting ScribblePrompt-UNet.

## H. Inference Runtime

**Setup.** We measure inference time for a random input with a scribble covering 128 pixels. We report mean and standard deviation of inference time across 1,000 runs on a single CPU and on a Nvidia Quatro RTX8000 GPU.

**Results.** We show performance results in Tab. 8. On a single CPU, ScribblePrompt-UNet requires  $0.27 \pm 0.04$  sec per prediction, enabling the model to be used in real-time even in low-resource environments. ScribblePrompt-UNet is faster than the baseline methods on a GPU. Unlike the transformer-based models, the inference time for each predic-

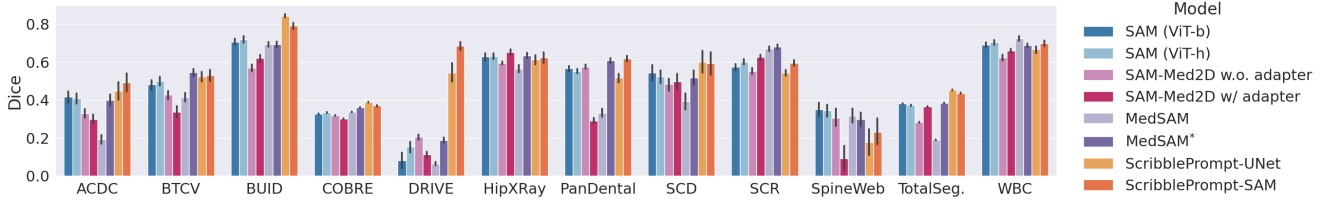


Figure 18. **Results with simulated bounding boxes by dataset.** Mean Dice after one simulated bounding box prompt. Among the evaluation datasets, bounding box prompts are the most effective for BUID, a breast ultrasound dataset. MedSAM\* indicates MedSAM with input images re-scaled to  $[0, 1]$  instead of the pixel normalization from [63]. Errorbars show 95% CI from bootstrapping.

Table 8. **Performance Summary.** We measure inference time separately on a single CPU and on an Nvidia Quatro RTX8000 GPU for a prediction with a random scribble input covering 128 pixels. We report mean and standard deviation across 1,000 runs. ScribblePrompt-SAM and MedSAM use the same architecture as SAM ViT-b. **Best** and **second best** are highlighted.

Architecture	Param.	CPU Runtime (sec)	GPU Runtime (ms)
SAM (ViT-h)	641M	130.79 ± 7.96	504.36 ± 57.72
SAM (ViT-b)	94M	13.59 ± 0.77	133.85 ± 24.26
SAM-Med2D w/ adapter	271M	1.23 ± 0.07	35.06 ± 12.88
SAM-Med2D w.o. adapter	91M	0.63 ± 0.02	24.86 ± 9.56
MIDeepSeg	3M	0.08 ± 0.02	65.75 ± 21.87
ScribblePrompt-UNet	4M	0.27 ± 0.04	1.96 ± 0.20

tion is does not depend on the number of of input interactions for ScribblePrompt-UNet.

## I. Ablations

We conduct two ablations of important ScribblePrompt design decisions: (1) synthetic label inputs used during training, and (2) types of prompts simulated during training. We report results on the validation splits of nine validation datasets that were unseen during training.

### I.1. Synthetic Labels

**Setup.** We trained ScribblePrompt-UNet and ScribblePrompt-SAM with different values of  $p_{synth}$ , the probability of sampling a synthetic label.

**Results.** Training with some synthetic labels improves both ScribblePrompt-UNet and ScribblePrompt-SAM’s performance on validation data from nine (validation) datasets not seen during training (Fig. 36, 37). For both ScribblePrompt-UNet and ScribblePrompt-SAM, training with 50% synthetic labels leads to the highest Dice on unseen datasets at inference time.

### I.2. Prompt Types

**Setup.** We evaluate ScribblePrompt-UNet models trained with different combinations of prompts, compared to the complete ScribblePrompt-UNet:

- **ScribblePrompt-UNet (scribbles)** trained on boxes and scribbles.
- **ScribblePrompt-UNet (clicks)** trained on boxes and clicks.
- **ScribblePrompt-UNet (random clicks)** trained on boxes and random clicks.

**Results.** Fig. 38 shows results for six different inference-time interaction procedures. ScribblePrompt-UNet trained with scribbles, clicks, and bounding boxes predicts segmentations more accurately than do ablated versions of ScribblePrompt-UNet.

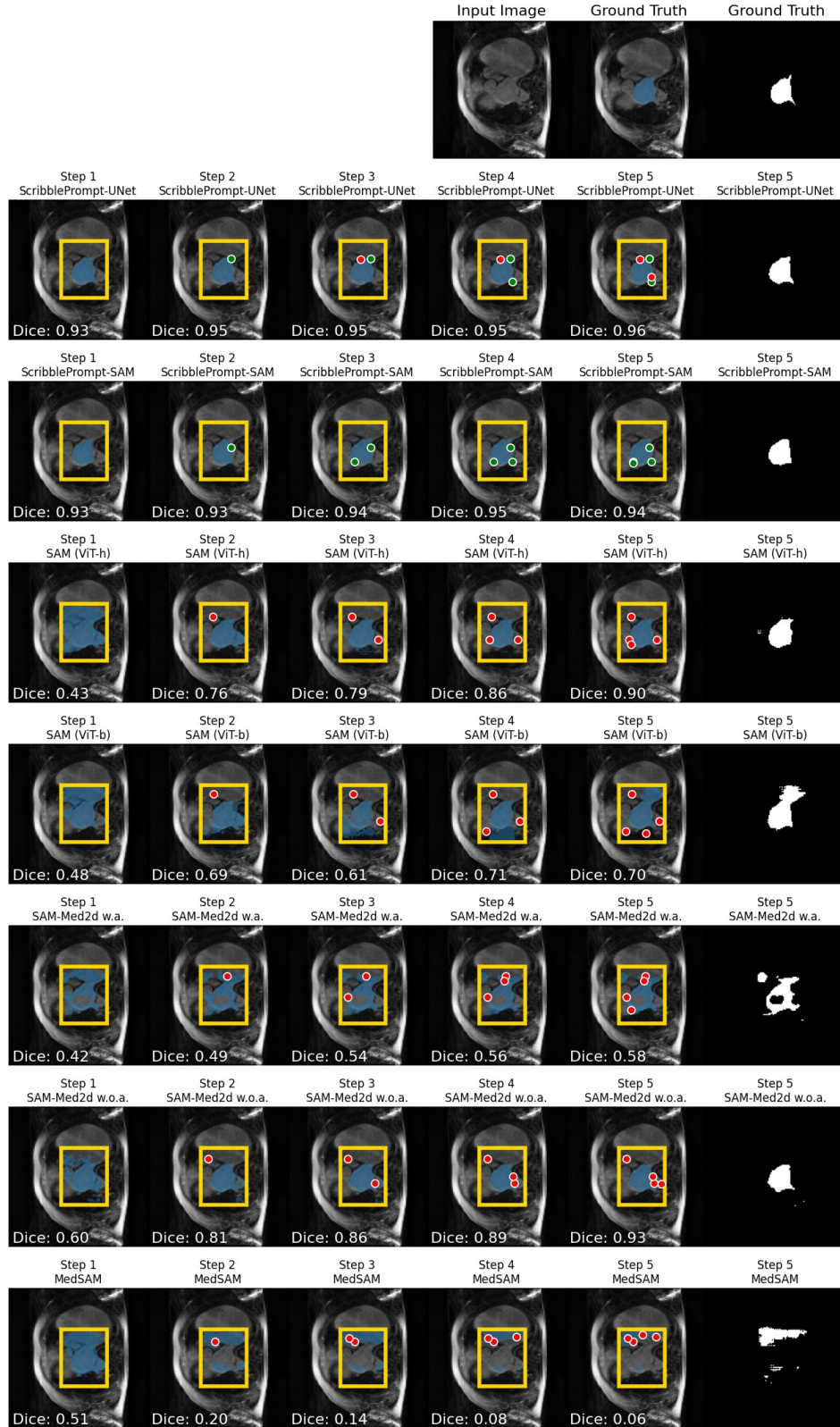


Figure 19. **Bounding box prompt with center correction clicks.** We simulate iterative interactive segmentation of the left ventricle in a cardiac MRI from the SCD dataset [105]. This label was seen during training but this dataset was not. ScribblePrompt models produce the highest dice predictions after a single bounding box prompt (first column) and are able to improve their predictions with additional corrections.

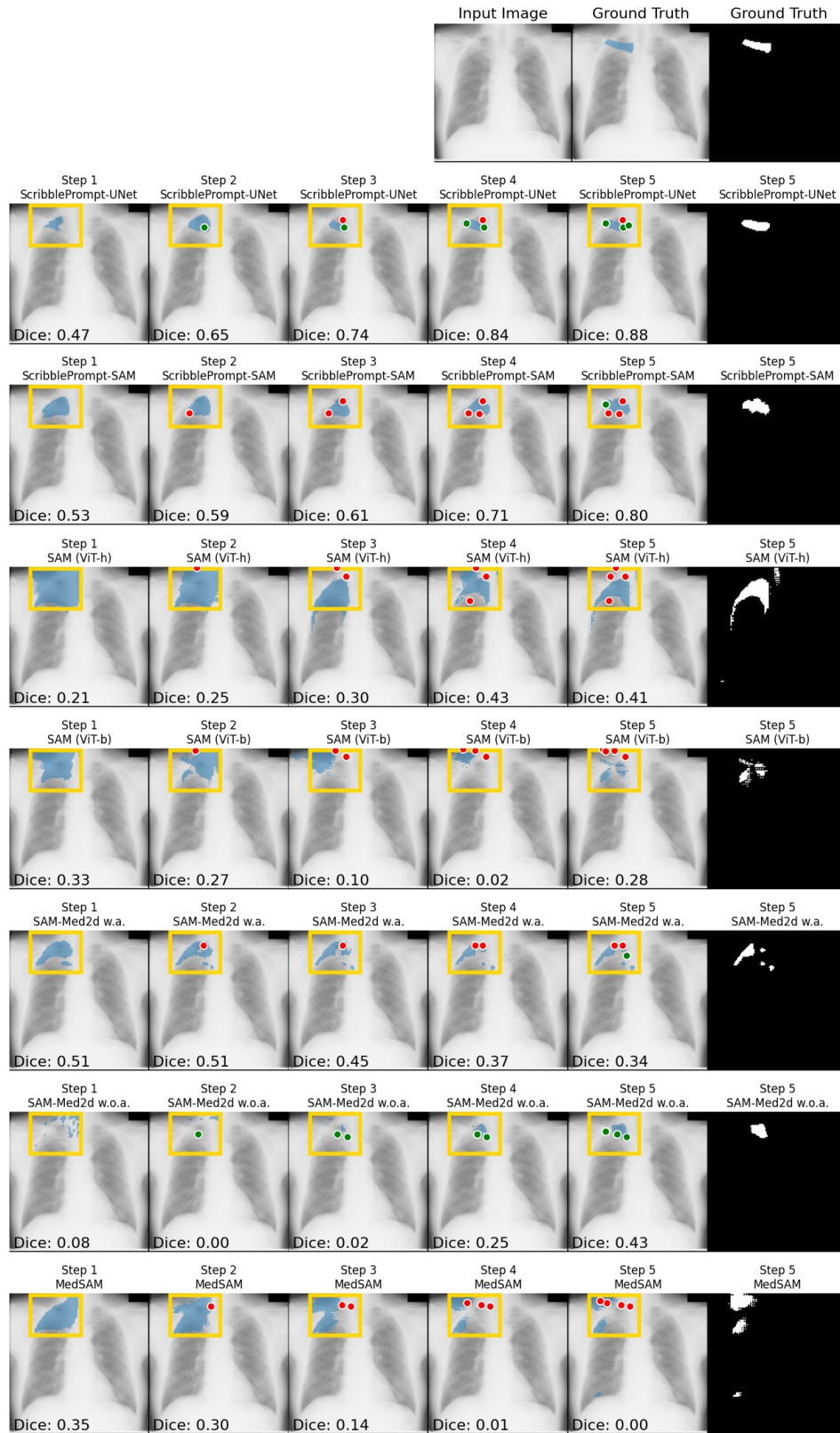


Figure 20. **Bounding box prompt with center correction clicks.** We show clavicle segmentation on an frontal chest X-Ray from the SCR dataset [128]. This dataset was completely held-out and this label was unseen during training. None of the methods are able to accurately segment the clavicle from a single bounding box prompt (first column). However, after a few correction clicks, ScribblePrompt-UNet and ScribblePrompt-SAM achieve 0.88 and 0.80 Dice, respectively.

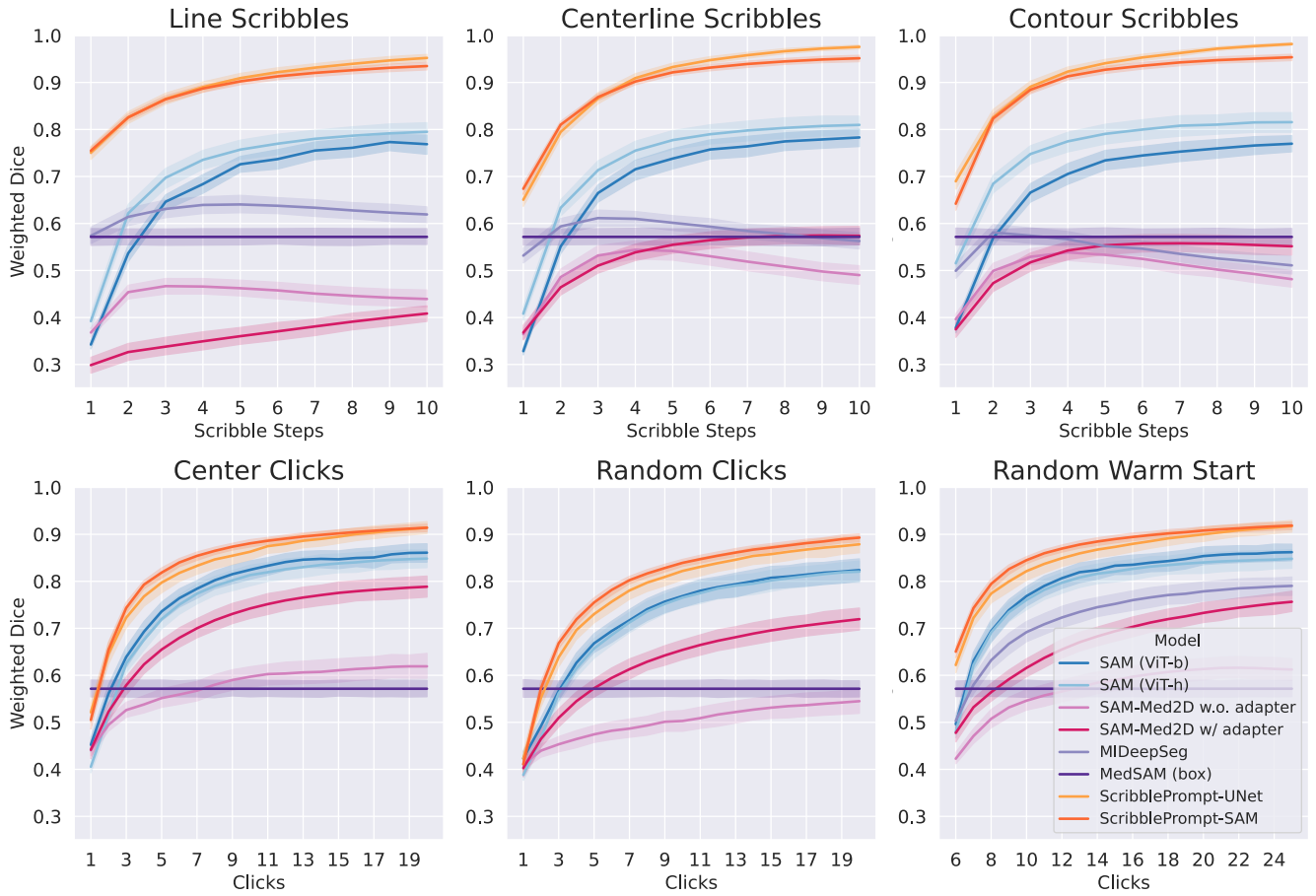


Figure 21. **Dice results with simulated scribbles and clicks.** We evaluate methods using three scribble procedures and three click procedures. We measure Dice averaged across twelve evaluation sets (the test splits of the nine validation and three test datasets), weighting each dataset equally. Shaded regions show 95% CI from bootstrapping.

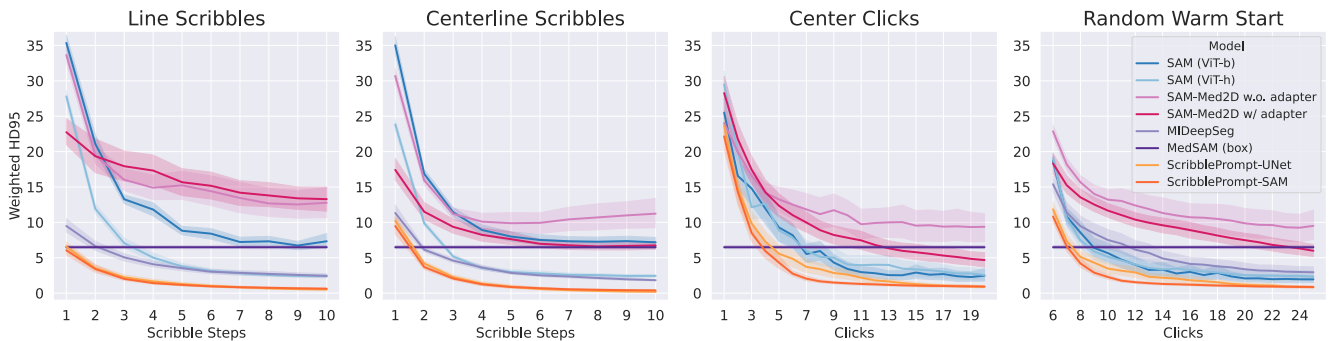


Figure 22. **HD95 results with simulated scribbles and clicks** We report HD95 for two scribble procedures and two click procedures. We measure HD95 averaged across twelve evaluation sets (the test splits of the nine validation and three test datasets), weighting each dataset equally. We exclude examples where the ground truth segmentation label was empty or the predicted segmentation was empty. Shaded regions show 95% CI from bootstrapping.

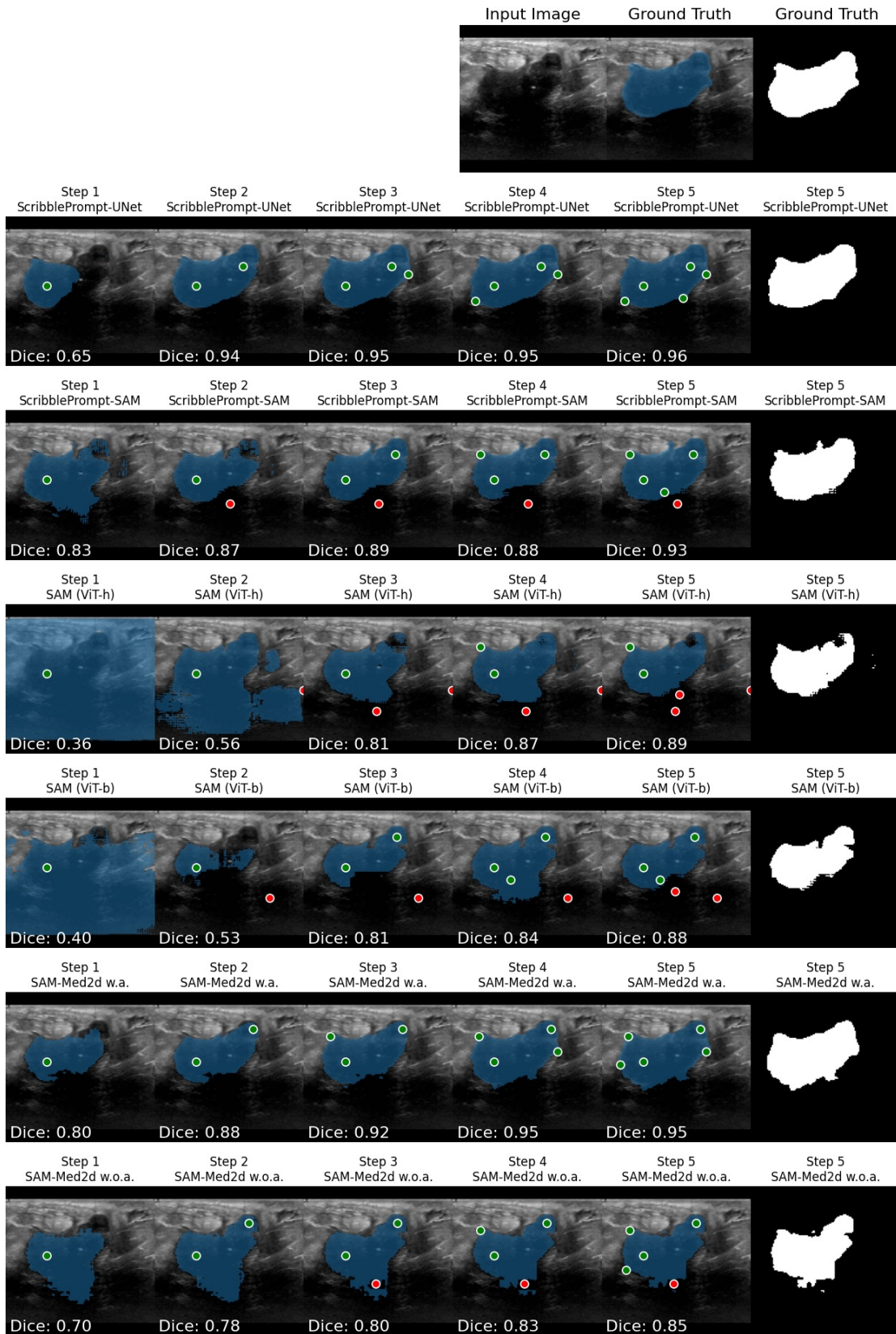


Figure 23. **Example predictions from center clicks.** We show an example of interactive segmentation of a malignant tumor in an Ultrasound image from the BUID [5] dataset. This dataset was unseen by ScribblePrompt models during training. We simulate an initial click in the center of the label followed by one correction click in the center of the error at each step.



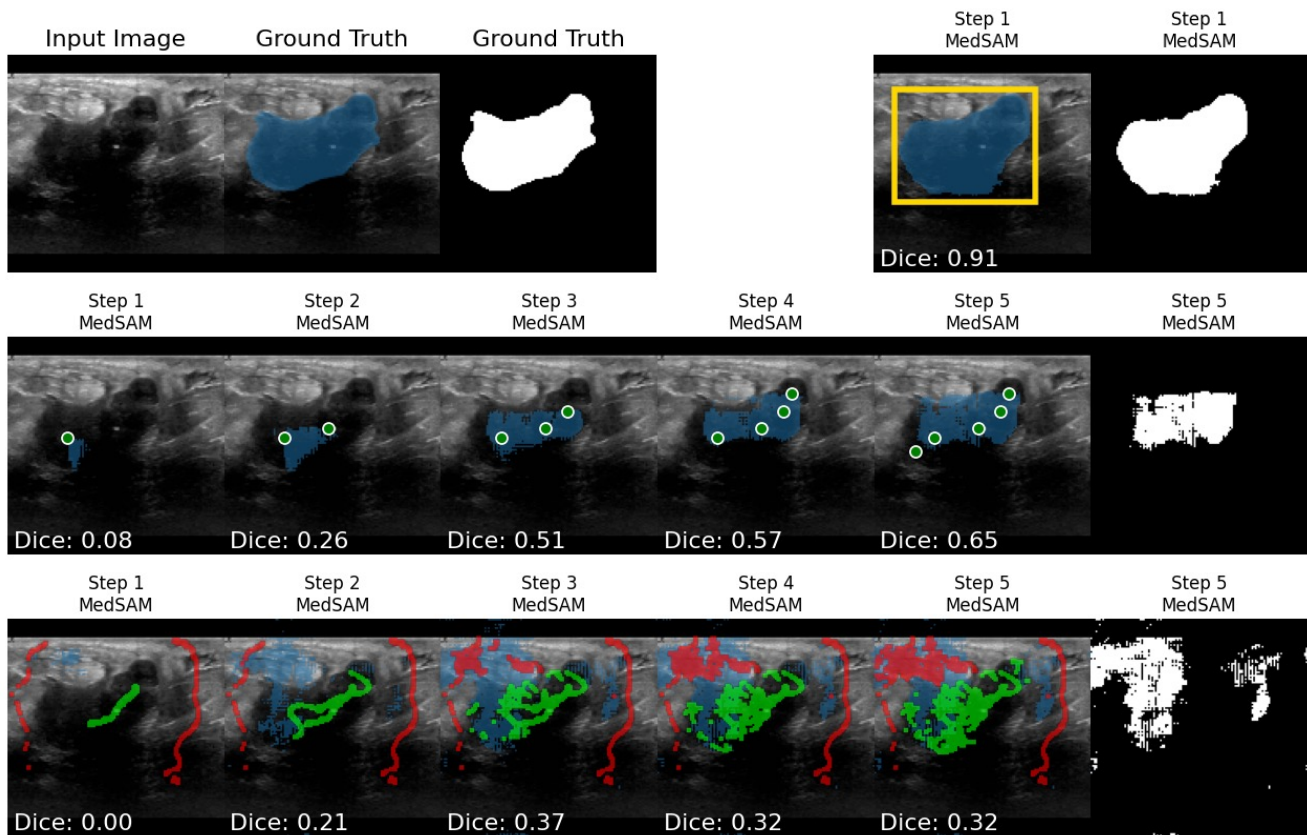


Figure 24. **MedSAM with bounding box, click, and scribble inputs.** We do not evaluate MedSAM with click and scribble inputs, which it was not trained for, because it produces poor segmentations with these inputs. Scribble thickness is enlarged for visual clarity.

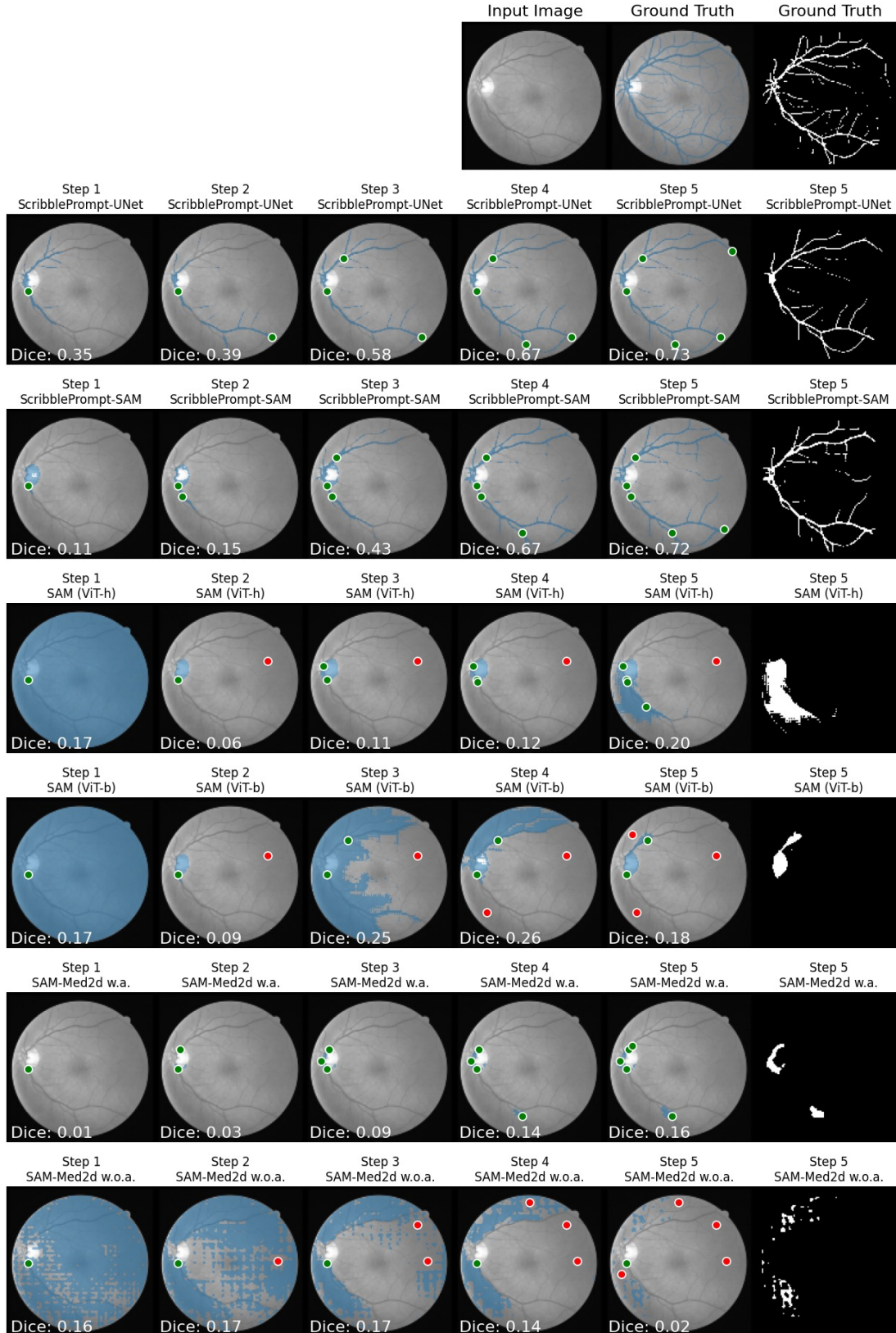


Figure 25. **Example predictions from center clicks.** We show an example of iterative interactive segmentation of retinal veins in a fundus photograph from the DRIVE dataset [125]. This dataset was unseen by ScribblePrompt models during training. The ScribblePrompt models are able to segment the retinal veins while baseline methods are not able to segment these thin structures.

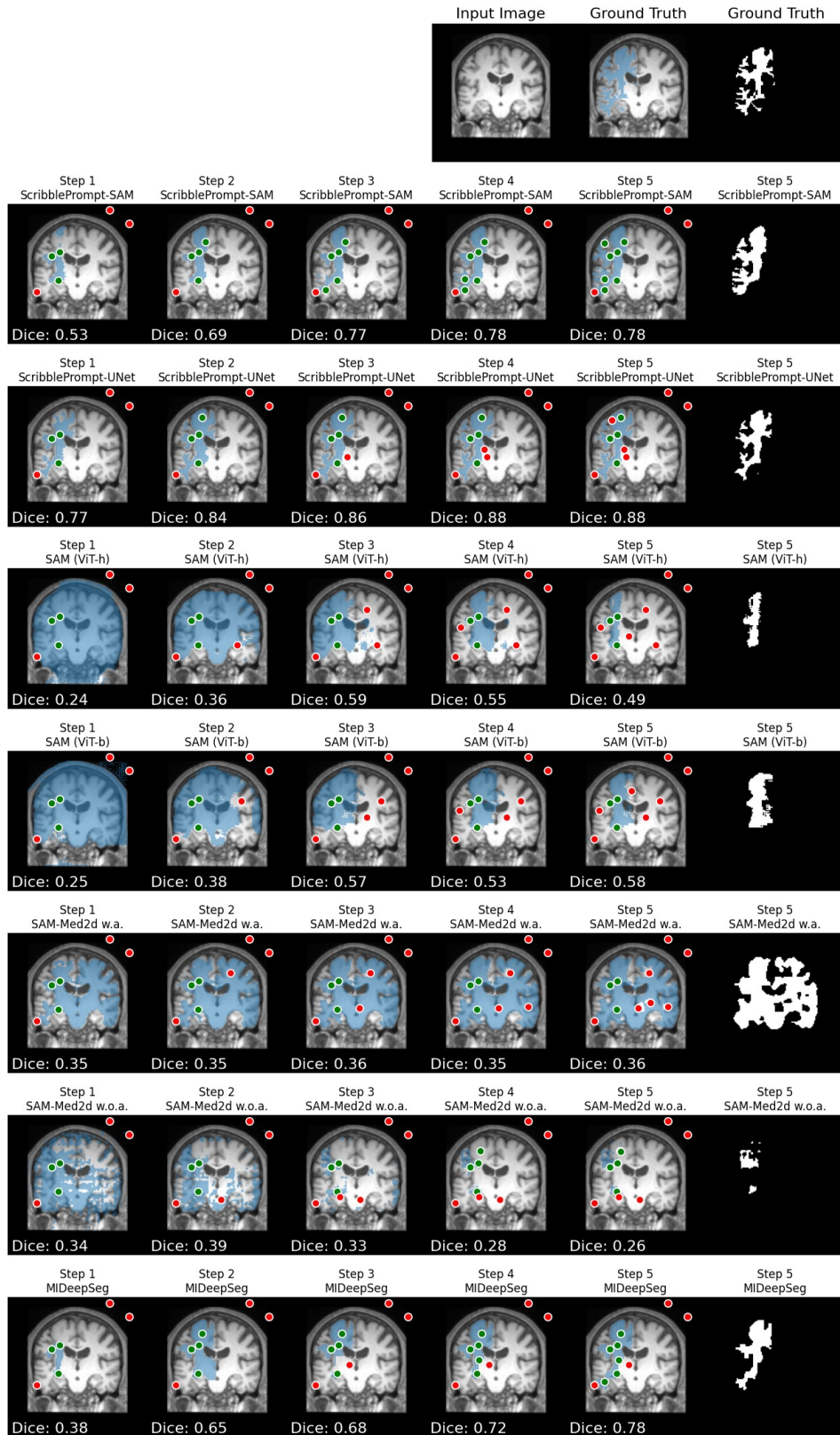


Figure 26. **Example predictions from random clicks and center correction clicks.** We show an example of white matter segmentation in a T1 brain MRI from the COBRE dataset [4, 29, 34]. This dataset was completely held-out from ScribblePrompt training and model selection. We simulate interactions following the warm start click protocol: we start with three positive and three negative random clicks, followed by one center correction click per step.

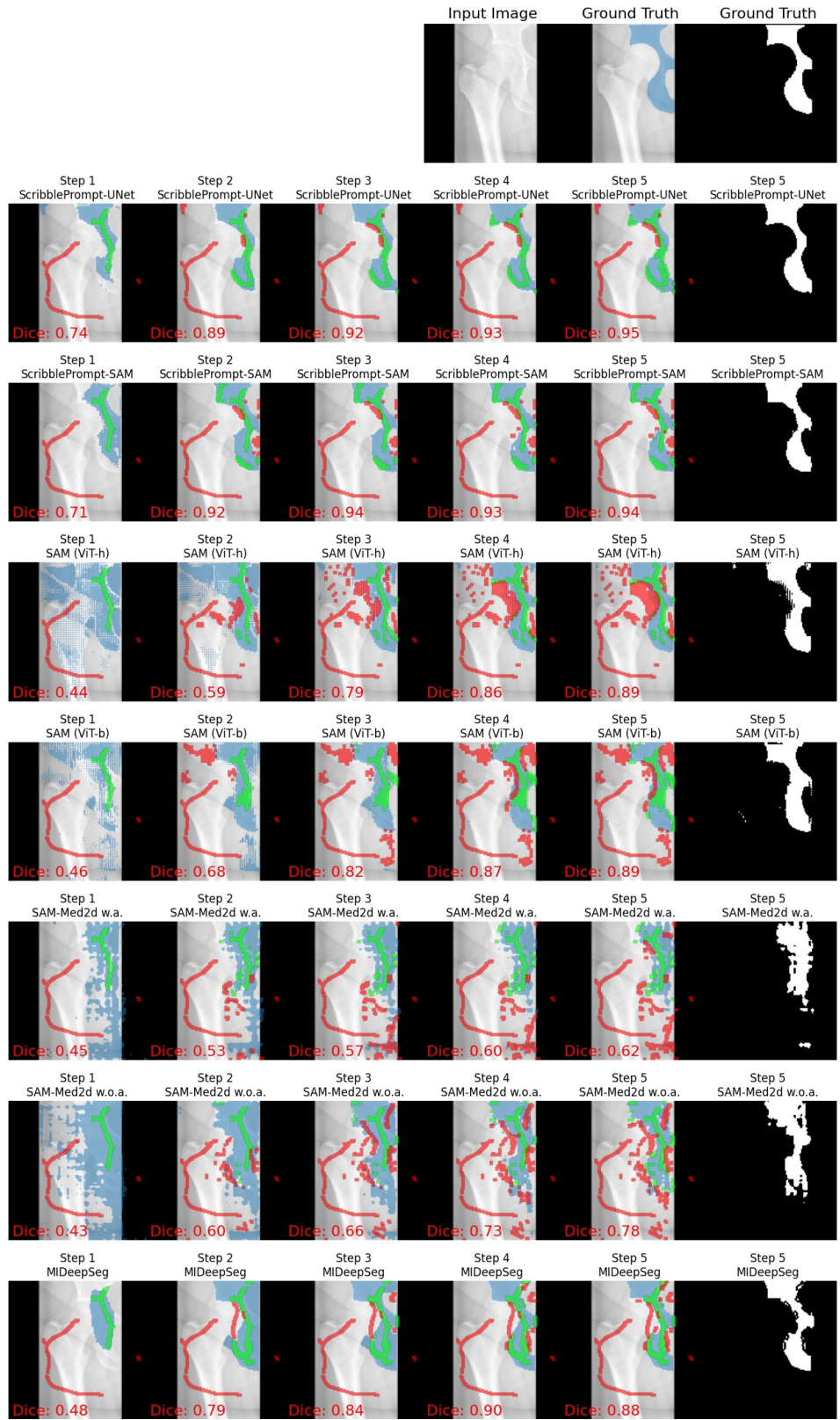


Figure 27. **Example predictions from centerline scribbles.** We simulate iterative interactive segmentation of the ilium in an X-Ray from the HipXRray dataset [43]. This dataset, label, and type of X-Ray was not seen by ScribblePrompt models during training. Correction scribbles were simulated separately for each method based on the error region of the previous prediction. ScribblePrompt models have the highest Dice predictions after 5 scribble steps. Scribble thickness is enlarged for visual clarity.

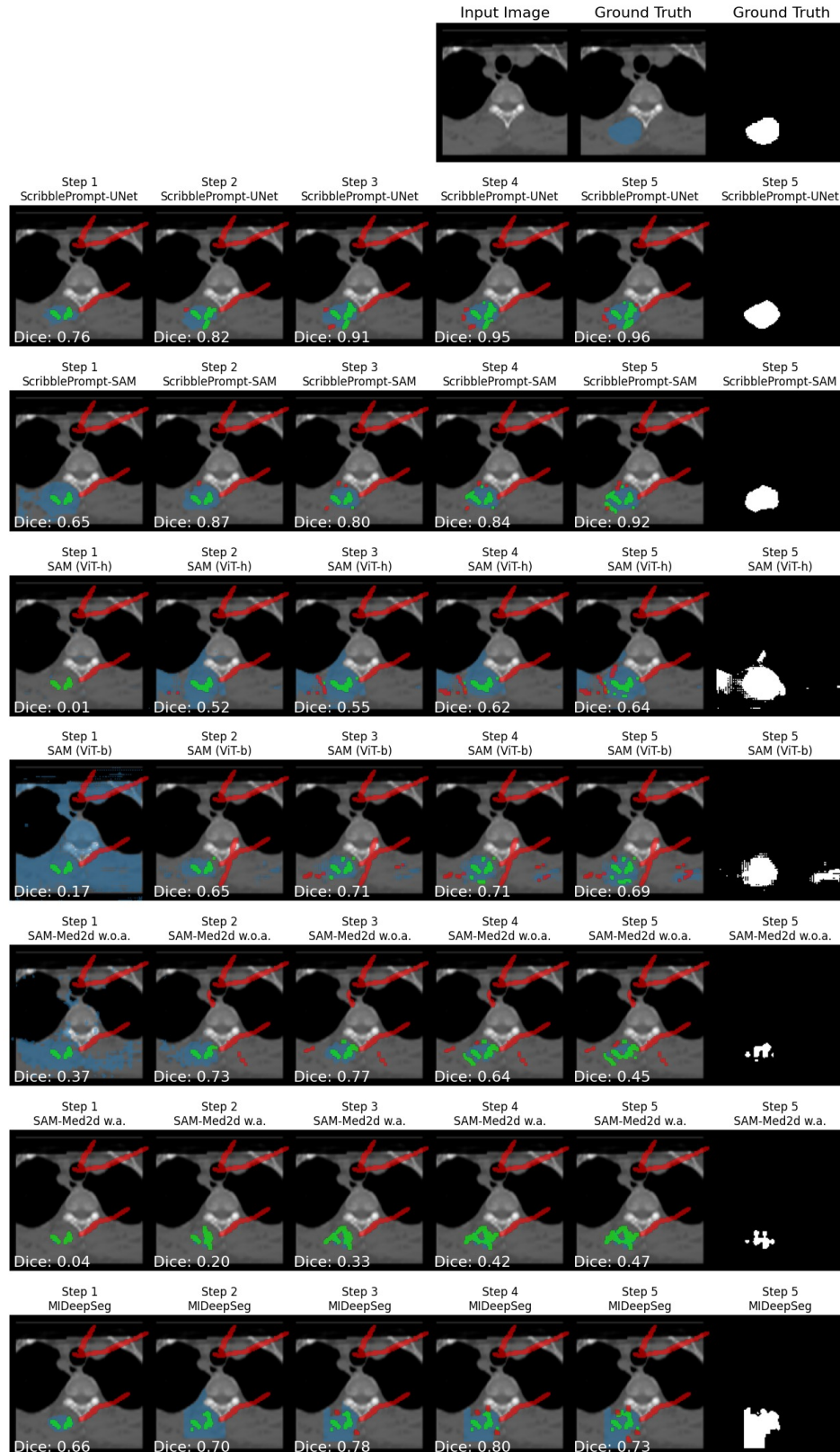


Figure 28. **Example predictions from line scribbles.** We simulate iterative interactive segmentation of the left autochthon muscle in a CT from the TotalSegmentator dataset [137]. This dataset was completely held-out and the label was unseen by ScribblePrompt models during training. This segmentation task is challenging because there is little contrast between the region of interest and surrounding tissue. ScribblePrompt models are able to accurately refine their predictions and achieve  $\text{Dice} \geq 0.92$  after 5 scribble steps. Scribble thickness is enlarged for visual clarity.

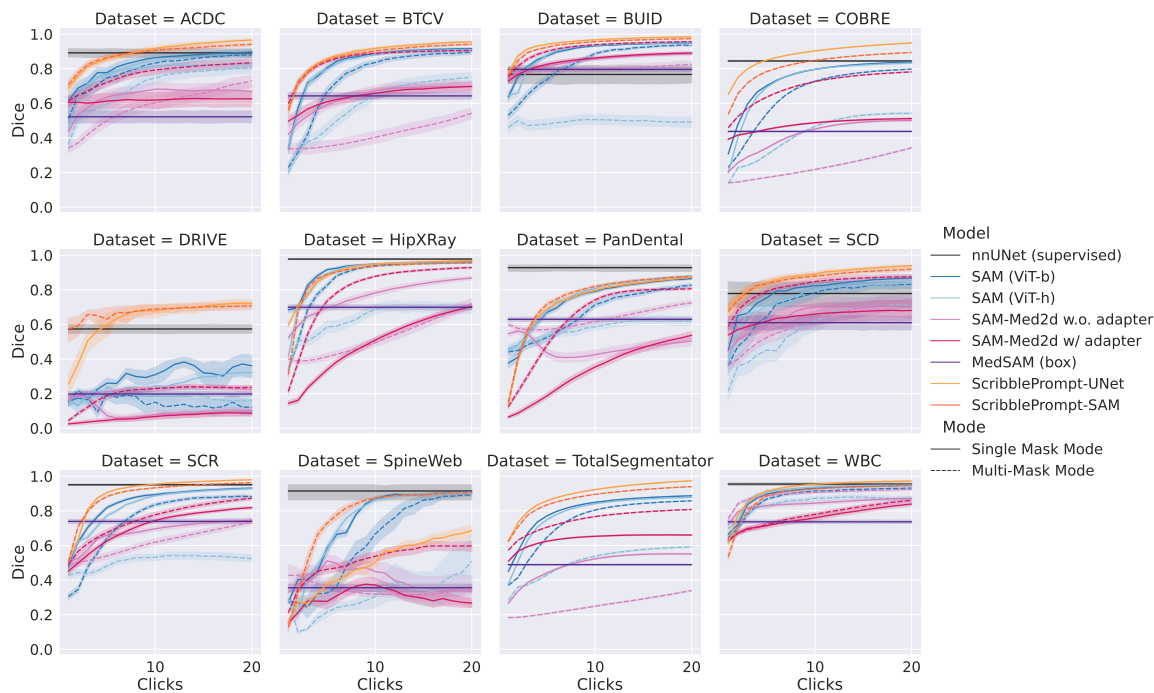


Figure 29. **Results by dataset with center clicks.** During the first step, one positive click is placed at the center of the largest component of the ground truth segmentation. In subsequent iterations, one (positive or negative) correction click is placed at the center of the largest component of the error region between the previous prediction and ground truth segmentation.

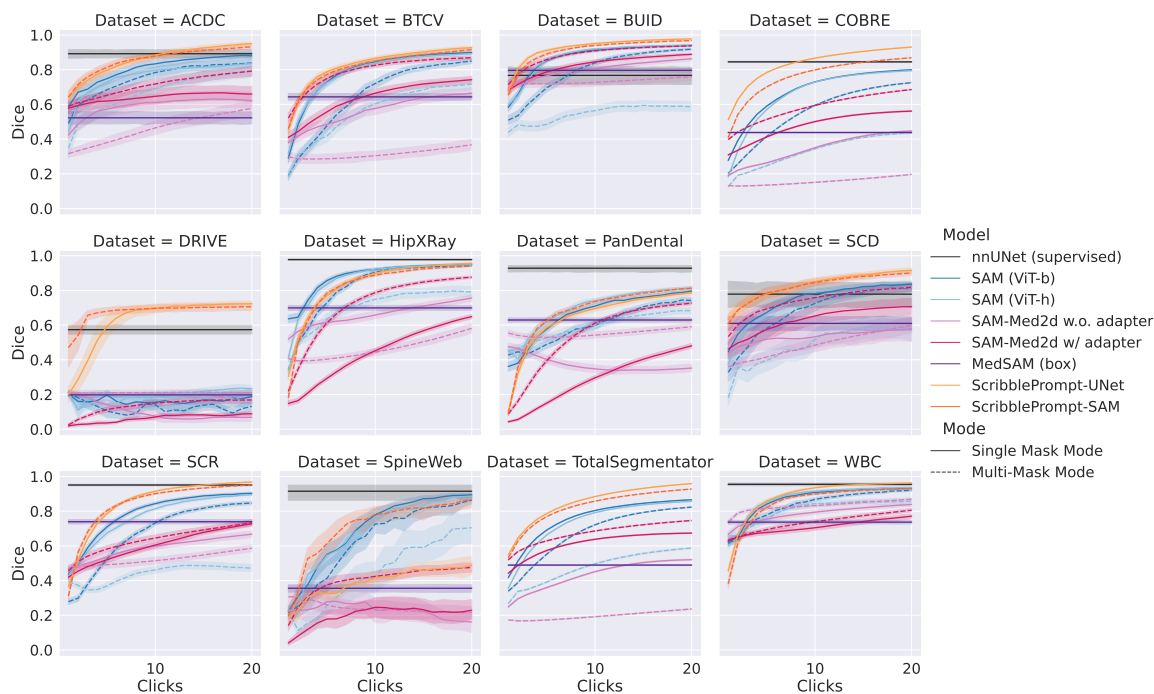


Figure 30. **Results by dataset with random clicks.** During the first step, one positive click is randomly sampled from the ground truth segmentation. In subsequent steps, one (positive or negative) correction click is randomly sampled from the error region between the previous prediction and ground truth segmentation.

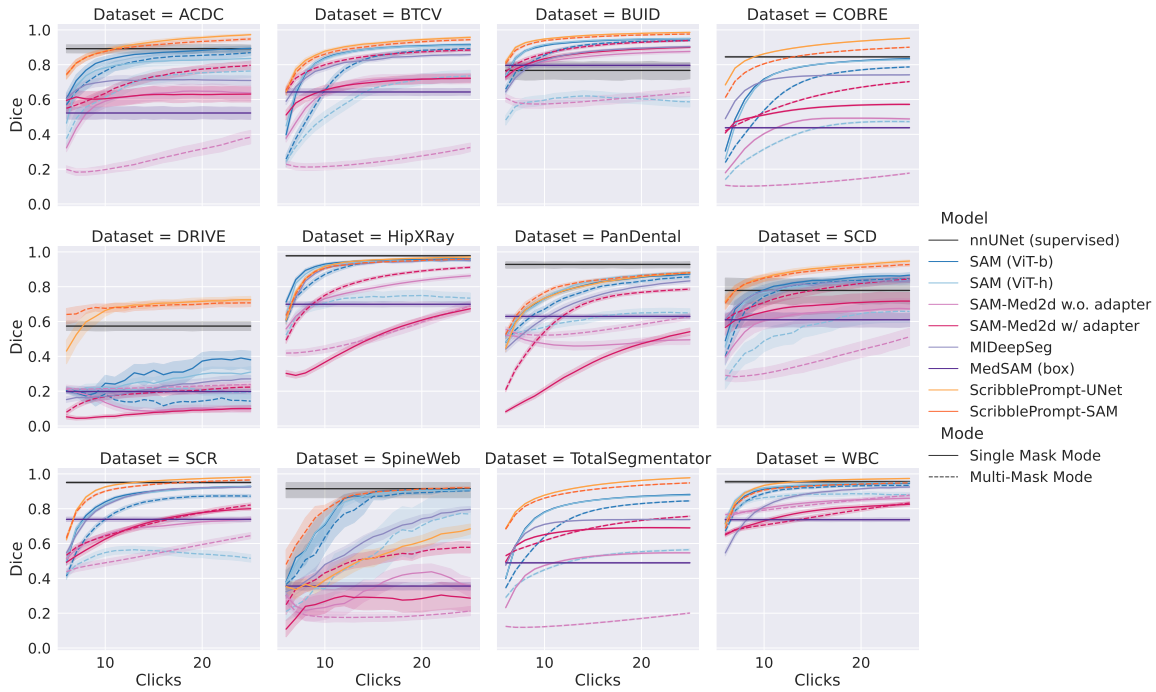


Figure 31. **Results by dataset with random warm start click procedure.** During the first step, three positive clicks are randomly sampled from the ground truth segmentation and three negative clicks are randomly sampled from the background. In subsequent steps, one (positive or negative) correction click is placed at the center of the largest component of the error region between the previous prediction and ground truth segmentation.

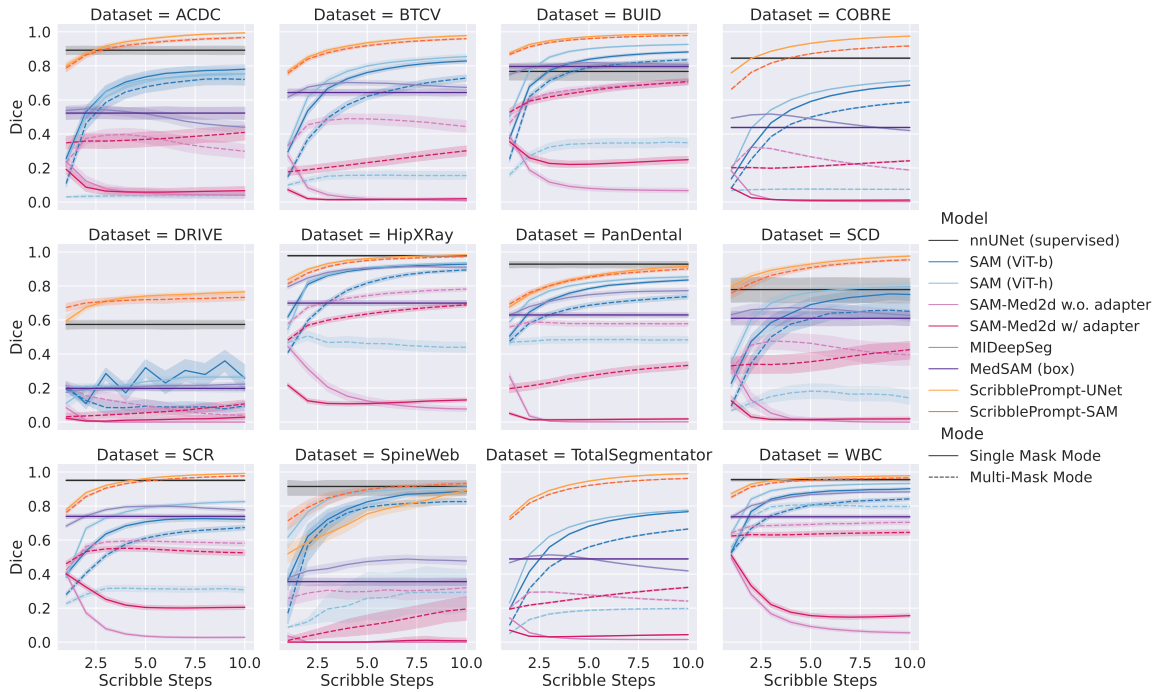


Figure 32. **Results by dataset with line scribbles.** During the first step we simulate three positive line scribbles and three negative line scribbles. In subsequent steps, we simulate one (positive or negative) correction line scribble based on the error region between the previous prediction and ground truth segmentation. Each line scribble covers a maximum of 128 pixels.

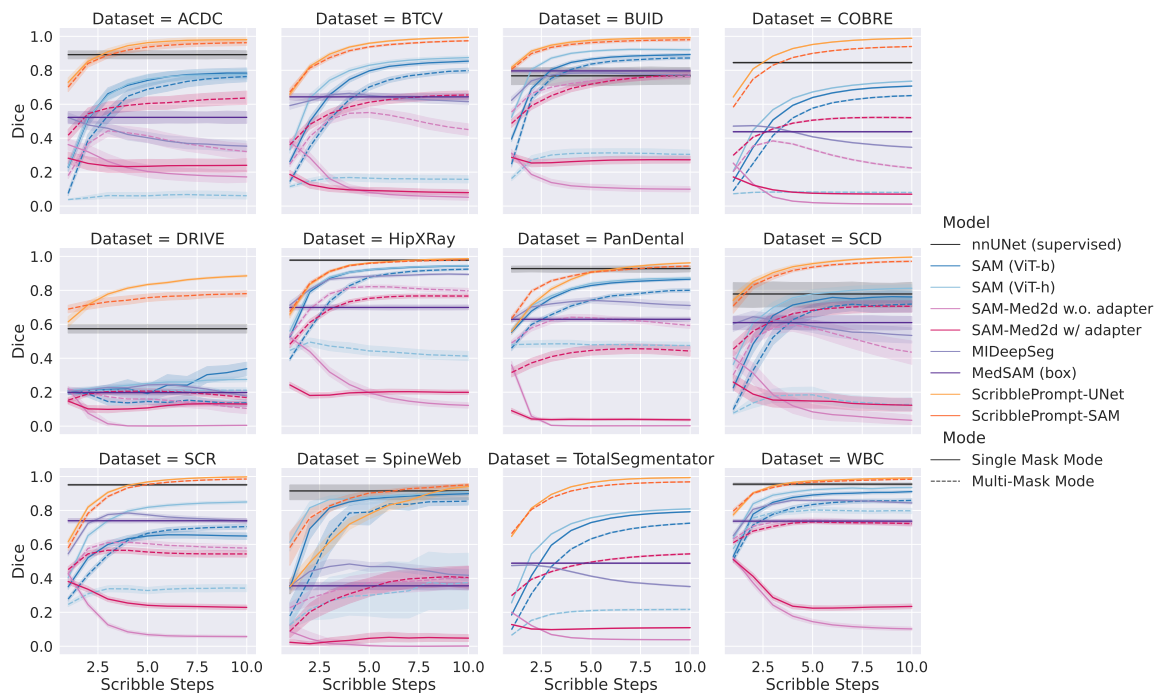


Figure 33. **Results by dataset with centerline scribbles.** During the first step, we simulate one positive and one negative centerline scribble. In subsequent steps, we simulate one (positive or negative) correction centerline scribbles based on the error region region between the previous prediction and ground truth segmentation. Each centerline scribble covers a maximum of 128 pixels.

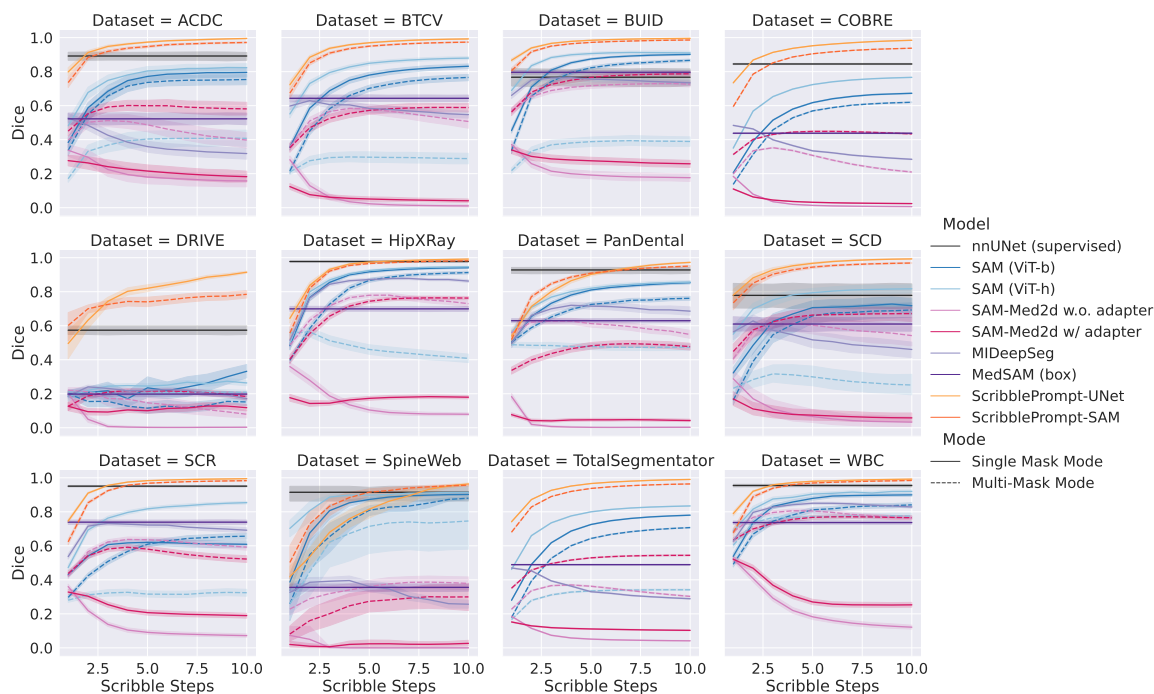


Figure 34. **Results by dataset with contour scribbles.** During the first step, we simulate one positive and one negative contour scribble based on the ground truth label. In subsequent steps, we simulate one (positive or negative) correction contour scribble based on the error region region between the previous prediction and ground truth segmentation. Each contour scribble covers a maximum of 128 pixels.



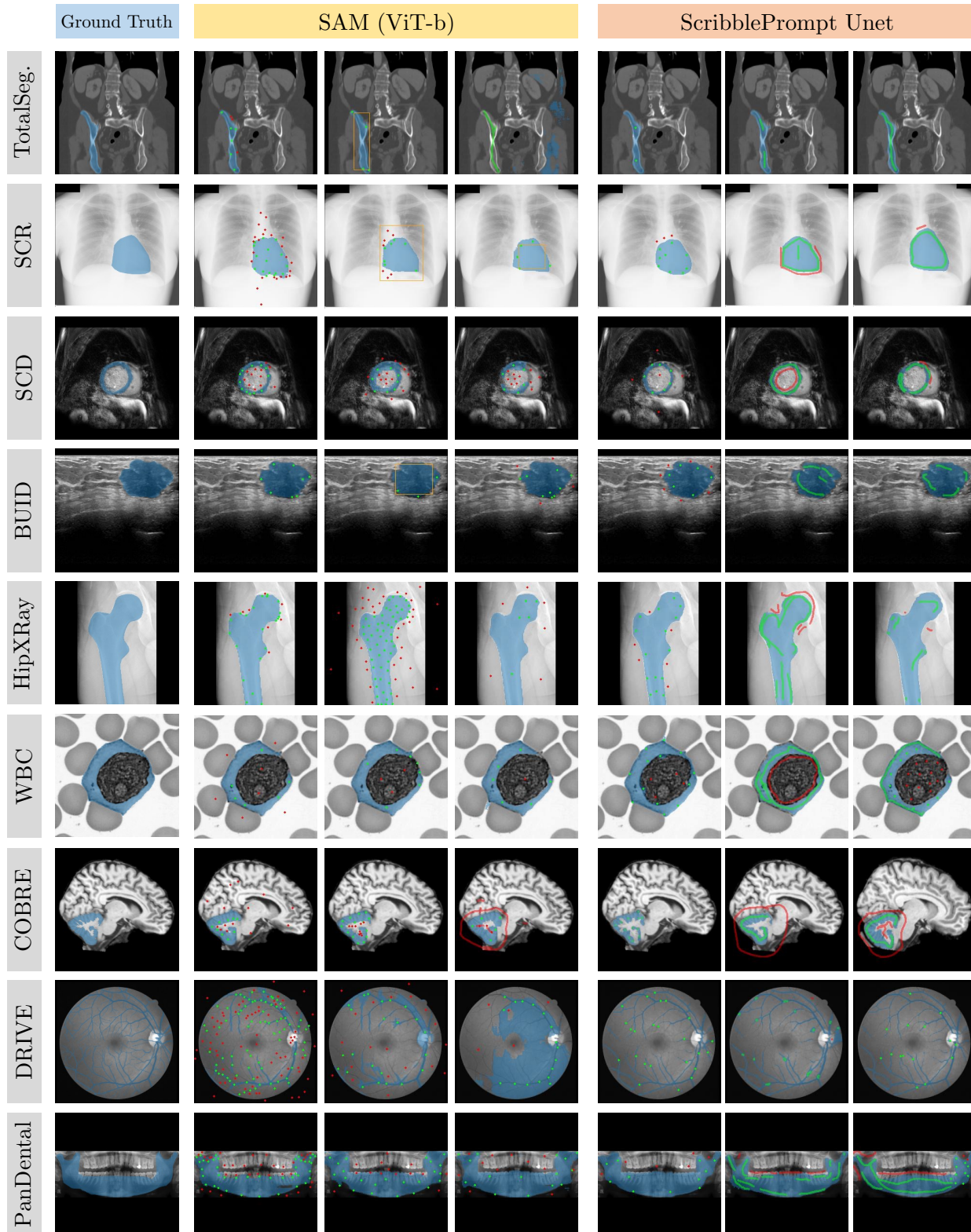


Figure 35. **Example segmentations and interactions from the user study.** We show predictions with interactions provided by three study participants for each of the nine segmentation tasks in the user study. For each example, we visualize positive scribble and click inputs in green, negative scribble and click inputs in red, bounding box inputs in yellow, and the predicted segmentation in blue. With SAM, study participants primarily used clicks. With ScribblePrompt, participants used a mix of scribbles and clicks. For the retinal vein segmentation task, participants preferred to use clicks with both models. Participants prompted SAM with denser clicks compared to ScribblePrompt.

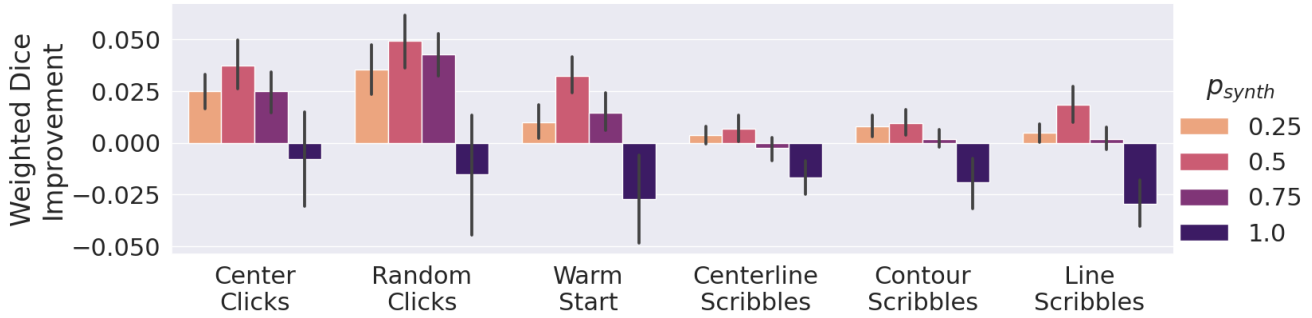


Figure 36. **Probability of synthetic labels during training for ScribblePrompt-UNet.** We report change in Dice relative to ScribblePrompt-UNet trained without any synthetic labels ( $p_{synth} = 0$ ). We show Dice after five steps of simulated interactions following six different (inference-time) interaction procedures. Errorbars show 95% CI.

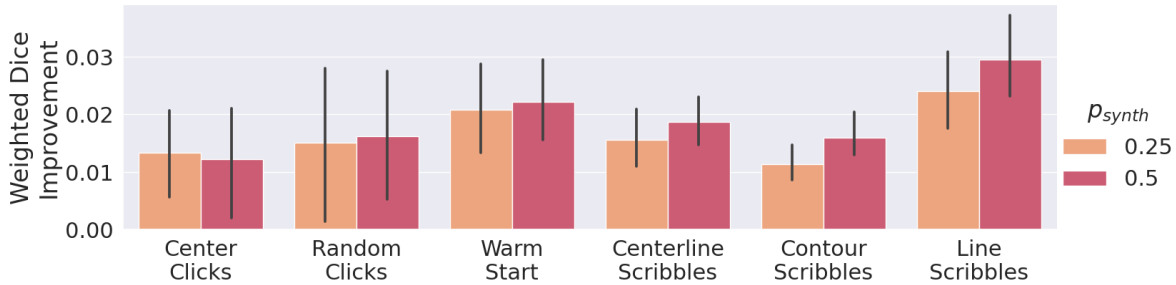


Figure 37. **Probability of synthetic labels during training for ScribblePrompt-SAM.** We report change in Dice relative to ScribblePrompt-SAM trained without any synthetic labels ( $p_{synth} = 0$ ). We show Dice after five steps of simulated interactions following six different (inference-time) interaction procedures. Errorbars show 95% CI.

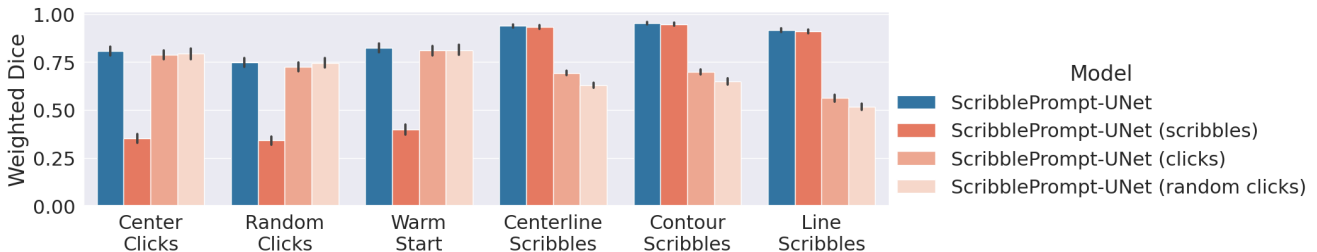


Figure 38. **Ablation of interactions during training.** We report Dice after five steps of simulated interactions following six inference-time interaction procedures. Error bars show 95% CI from bootstrapping.